

UNSW AUSTRALIA

SCHOOL OF MECHANICAL AND  
MANUFACTURING ENGINEERING

**Development of an Automated  
Magnetic Silica Bead Based  
DNA/RNA Extractor**

**Jarrod Herbert Stilp**  
z3460979

Bachelor of Engineering, Mechatronic Engineering

October 2016

Supervised by Associate Professor Jayantha  
Katupitiya

# **Development of an Automated Magnetic Silica Bead Based DNA/RNA Extractor**

**Jarrod Herbert Stilp**

Submitted for the degree of Bachelor of Engineering,

Mechatronic Engineering

October 2016

## **Abstract**

This work has integrated into the AusDiagnostics Gene-Plex platform a number of key capabilities required for performing the extraction of DNA/RNA from a human sample utilizing super paramagnetic silica beads. By considering the factors effecting a designs thermal stability, hardware capable of maintaining a stable steady state, driven temperature was developed. Through guided and iterative design, the Ferrotect 9500-035-085 B was selected for use in a pair as the heating element. Numerical simulation and experimental verification found these modules capable of exceeding the response requirements of the system. A PID controller was developed to drive the system to the required set point and was found, following calibration, to meet the stipulated requirements with a time response of 81.16 seconds and a steady state error of  $0.083^{\circ}\text{C}$ . Despite a discrete time controller being developed via the direction analytical method and validated via simulation, a software bug prevented the full experimental verification from being conducted. Via the investigation completed and preliminary experimental results, an effective means of magnetic separation has been determined.

# Certificate of Originality

I, Jarrod Herbert Stilp, hereby declare that this submission is my own work and to the best of my knowledge it contains no materials previously published or written by another person, or substantial proportions of material which have been accepted for the award of any other degree or diploma at UNSW or any other educational institution, except where due acknowledgement is made in the thesis. Any contribution made to the research by others, with whom I have worked at UNSW or elsewhere, is explicitly acknowledged in the thesis.

I also declare that the intellectual content of this thesis is the product of my own work, except to the extent that assistance from others in the projects design and conception in style, presentation and linguistic expression is acknowledged.

Signed .....

Date .....

# Acknowledgements

I would like to thank the following people for their support during the completion of this work.

Associate Professor Jayantha Katupitiya, for the valuable feedback during the completion of the work along with allowing me to pursue a topic within which I have great interest.

To the staff of AusDiagnostics of facilitating the requirements of this work and aiding their willingness to offer advice and knowledge throughout the year.

Sorenson Engineering, for efforts to manufacture the final product ahead of schedule and the great advantage this gave. Also to Julius and John for their invaluable advice and expertise in details of designing for manufacture and aiding me to get it right the first time.

Finally to my family, my parents Michael and Michelle, brother Nicholas and girlfriend Allie, thank you for your support throughout the year and for helping me to stay focused despite the unplanned moments.

# Contents

<b>Abstract</b>	ii
<b>Certificate of Originality</b>	iii
<b>Acknowledgements</b>	iv
<b>1 Introduction</b>	1
1.1 Background . . . . .	1
1.1.1 The Extraction Process . . . . .	4
1.2 Aim . . . . .	8
1.3 Scope . . . . .	8
1.3.1 Mechanical . . . . .	8
1.3.2 Electronic . . . . .	10
1.3.3 Software . . . . .	11
<b>2 Literature Review</b>	12
2.1 Heating . . . . .	12
2.2 Cooling . . . . .	15
2.3 Controllability . . . . .	16
2.4 Temperature Sensors . . . . .	18
2.5 Temperature Sensing . . . . .	19

<b>Contents</b>	<b>vi</b>
2.6 Controller Design . . . . .	21
2.7 Magnetic Separation . . . . .	22
<b>3 Methodology</b>	<b>25</b>
3.1 Processor Module . . . . .	26
3.1.1 Hardware . . . . .	26
3.1.2 Temperature Controller . . . . .	27
3.1.3 Magnetic Separation . . . . .	38
<b>4 Results and Discussion</b>	<b>39</b>
4.1 Processor Module . . . . .	40
4.1.1 Hardware . . . . .	40
4.1.2 Final Mechanical Design . . . . .	57
4.1.3 Processor Module Assembly . . . . .	64
4.1.4 Temperature Controller . . . . .	71
4.1.5 Magnetic Separation . . . . .	88
<b>5 Conclusions</b>	<b>93</b>
<b>6 Future Work</b>	<b>96</b>
<b>References</b>	<b>97</b>
<b>A CFD Simulation Convergence Data</b>	<b>101</b>

# List of Figures

1.1	High-Plex Platform. . . . .	4
1.2	Extractor deck layout. . . . .	5
1.3	Extraction cassette tubes. . . . .	7
2.1	Thermoelectric Module Application. . . . .	14
3.1	Open loop plant valiation Simulink Model. . . . .	29
3.2	Unity feedback system. . . . .	32
3.3	Controller valiation Simulink Model. . . . .	36
3.4	Temperature Measured Tubes. . . . .	37
4.1	Thermal Insulation Concepts. . . . .	42
4.2	CFD Results - Refined Design. . . . .	54
4.3	CFD Results - Spatial Variations of Temperation. . . . .	55
4.4	CFD Results - Thermal Losses from Thermal Region to Carrier. . . . .	56
4.5	Design for Carrier Location on Thermal Region. . . . .	58
4.6	Cassette tube fit within Carrier and Thermal Region. . . . .	60
4.7	Heat sink final design. . . . .	61
4.8	Processor Module Exploded Rendering. . . . .	64
4.9	Processor Module Components. . . . .	65
4.10	TEC Module connection. . . . .	66
4.11	Heat sink thermal paste application. . . . .	67

---

4.12 Heat sink component assembly. . . . .	68
4.13 Thermistor Preparation. . . . .	68
4.14 Thermistor Placement. . . . .	69
4.15 Thermal Region and Board Assembly. . . . .	70
4.16 Assembled Processor Module. . . . .	71
4.17 Plant Identification Setup. . . . .	72
4.18 Full System Response to Step Input. . . . .	73
4.19 Plant Response to Step Input. . . . .	74
4.20 Plant validation simulation. . . . .	75
4.21 Controller Verification Experimental Setup. . . . .	78
4.22 Temperature Sensor Data - 60°C Setpoint. . . . .	79
4.23 Temperature Sensor Data Key Values - 60°C Setpoint. . . . .	80
4.24 Temperature Sensor Data Key Values - calibrated 63.2°C Set-point. . . . .	81
4.25 Discrete Plant Transfer Function Pole Zero Map. . . . .	83
4.26 Discrete Controller Simulation. . . . .	85
4.27 Halbach Array Flux Diagram. . . . .	89
4.28 Halbach Array Jig. . . . .	90
4.29 Halbach Array Jig - K=1. . . . .	91
4.30 Processor Module Magnet Positioning. . . . .	92
A.1 Convergence Plot for Refined Design CFD. . . . .	101

# **Chapter 1**

## **Introduction**

### **1.1 Background**

Within the healthcare industry, there is a continuous need for fast and reliable diagnostics of pathogens within patients. Identifying the presence of pathogens responsible for disease in a patient allows the appropriate preventive or corrective action to be taken and represents a crucial step in treating or preventing illness. This thesis was conducted for the benefit of and in collaboration with AusDiagnostics Pty Ltd.

Successful diagnostics, within the context of this thesis, can be summarised in three overall stages. Namely these are extraction, amplification and finally, analysis. This thesis concerns itself only with extraction. It should be noted that not all pathogen analysis and/or commercial diagnostic processes follow these steps strictly, however the processes and technologies applied by AusDiagnostics follow this procedure. The stages of this procedure may be summarised as follows:

1. Extraction To begin the diagnosis, a clinical sample is obtained from the patient.

This sample may consist of cerebrospinal fluid, faecal matter, urine or others, depending on the disease to be diagnosed. These samples contain the target DNA or RNA which will later be analysed to determine the presence of the pathogen and hence disease. They also contain a number of inhibitors to the process of amplification and analysis. Extraction is the process of removing said inhibitors and retaining only the target DNA or RNA. The result is referred to as a clean sample.

2. Amplification Amplification takes the clean sample and by one of many methods increases the overall count of the DNA. This may be with the intention of allowing multiple targets to be detected or to increase the sensitivity of the analysis.

3. Analysis Analysis uses one of many available methods to search for the presence of biomarkers within the amplified clean sample. The presence of the biomarker indicates the result of the diagnosis.

AusDiagnostics currently supplies customers with the instruments and chemical products required to complete stages two and three (amplification and analysis) of the diagnosis. This requires customers to purchase extraction equipment from alternative suppliers and represents a significant weakness and loss of profit. Research and development conducted by AusDiagnostics has determined that the optimal extraction method, when considering speed and efficiency, is super-paramagnetic bead based extraction. The beads utilised are of the shell-core variety. The core is composed of an iron oxide, which provides the super paramagnetic properties required for physical manipulation of the beads via a magnetic field. The shell is comprised of silica which, via chemical modification has the propensity to bond DNA and RNA to the bead surface. The techniques developed by

researchers at AusDiagnostics utilising the magnetic silica beads have been validated and verified via manual operation. This thesis concerns itself with the automation of the developed extraction process, to produce a commercially viable robotic instrument. This instrument will be referred to as the Gene-Plex Extractor.

The extraction process to be automated has a number of notable requirements. These include liquid handling via precise pipetting, including mixing and liquid transfer. Also required is manipulation of the magnetic silica beads to separate the bonded and hence captured target DNA or RNA, along with heating to a specified, constant temperature to act to increase the rate of the chemical processes. The automation of the extraction process will be achieved by integrating the required capabilities into the robot produced by AusDiagnostics to conduct the amplification stage of diagnosis. The instrument, based of the Gene-Plex platform and sold as the High-Plex Processor, is pictured in it's current application in Figure 1.1. The Gene-Plex platform is essentially a liquid handling robot. The robot carries out the amplification stage by precisely pipetting and transferring liquid mixtures between the tubes and instruments on the deck, using disposable tips. Each individual assay (an analysis conducted to determine the presence and amount of a substance within a volume) utilises an individual layout of components on the robots deck. This makes the platform highly configurable for differing setups.



Fig. 1.1: The Gene-Plex liquid handling robot platform, as implemented as the High-Plex Processor.

### 1.1.1 The Extraction Process

In order to allow the aim and scope of the work to be clearly defined, a condensed overview of the extraction process developed by AusDiagnostics is presented. It should be noted that unless explicitly stated, all operations are to be automated.

The extraction process requires that the clinical sample undergoes a number of chemical steps across different locations on the robot. To aid in understanding the liquid handling involved, Figure 1.2 displays the important sites on the deck. The process will begin with the operator manually loading 24 individual clinical samples into the location labelled “Clinical Sam-

ples". In order to conform to existing products used by customers, it is then required that the chemical processing takes place in the locations labelled "Samples". In order to transfer the liquid between locations, the robot will pick up 1000 $\mu$ L tips from the locations marked "Tips".

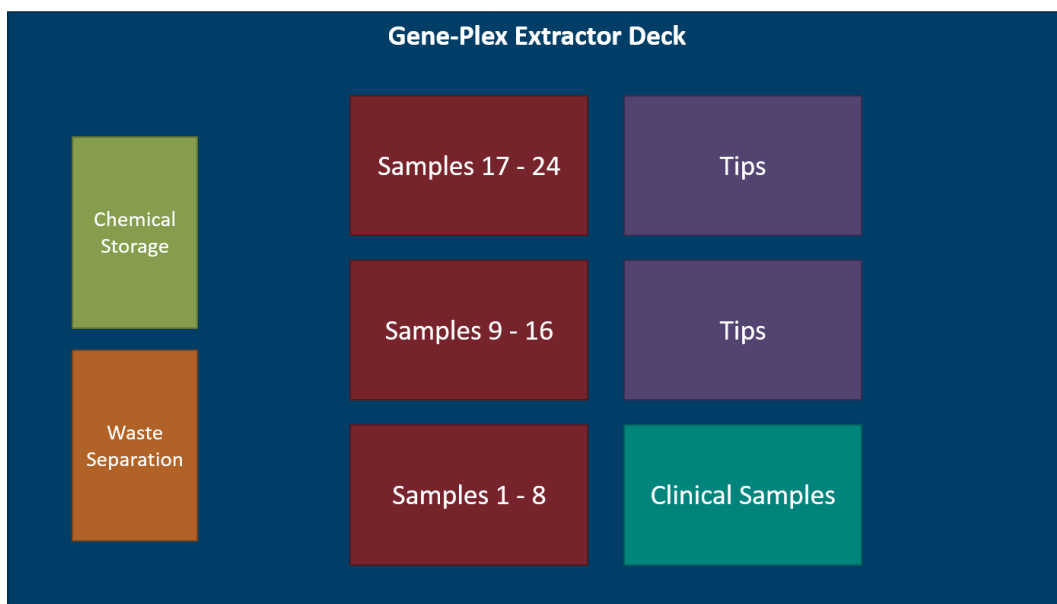


Fig. 1.2: The layout to be used for the Gene-Plex Extractor.

The sample processing locations must accept modules that fit within the standard block size (SBS) format. These blocks are required to each accept 8 cassettes, one for each sample (pictured in Figure 1.3). Each cassette includes 6 tubes, which will be the site of a particular chemical reaction in order to extract the target DNA and RNA:

1. 500 $\mu$ L of clinical sample is pipetted into tube location 2, as marked in Figure 1.3. Within this tube as supplied by AusDiagnostics, there will already be 10 $\mu$ L of magnetic bead mixture along with 440 $\mu$ L of lysis buffer. The lysis buffer will destroy the cell walls, releasing the target

DNA or RNA to be bound to the magnetic silica beads. This process is required to take place at 60°C in order to increase the rate of reaction. Due to the low volume of liquid in this step, it is to be completed in one of the 1mL low profile tubes. This aids with liquid handling precision.

2. The target DNA or RNA is now bound to the beads, which are suspended in the waste liquid (supernatant). In order to capture only the bead suspension, the entire liquid mixture is aspirated via the pipette tip and subsequently moved to the location marked "Waste Separation". In this location, a magnetic field is to be applied to capture the magnetic silica beads within the pipette tip. While captured, the supernatant must then be expelled into a waste container in this location. The tip now contains only the magnetic beads with bound targets.
3. Despite the supernatant having been expelled, there will still be a significant amount of waste retained on the bead surface. To remove this and clean the beads, a sequence of 3 wash steps must then occur in tube locations 1, 5 and 6. To achieve this, the beads are first re-suspended in the tube, which contains 800 $\mu$ L of a particular wash buffer. The suspension must then be mixed via pipetting in order to ensure the bead surface is properly exposed. The entire liquid mixture is then aspirated once again and transferred to the waste location, where via the same method as step 2, the waste liquid is disposed of while the beads are retained. This process is repeated 3 times in the tubes noted above to ensure no waste matter clings to the bead surface.
4. With the beads now clean and still bound to the target, the mixture is transferred to location 3 of the cassette. The elution buffer is used to

break the bond between the target DNA and RNA and the magnetic silica beads. This process is also required to be completed at 60°C to reduce the time required. Following this step, the target DNA or RNA of interest is now contained within the elution buffer, along with the magnetic silica beads which are now waste.

5. The final step is to capture only the target DNA or RNA within the elution buffer, leaving behind the magnetic beads. This is required to take place in tube location 4. This is a low volume reaction, containing only 100 $\mu$ L of elution buffer and is therefore completed in the final small profile tube. The pipette must then aspirate this mixture, following bead removal, and contain only the elution buffer and target mixture required for amplification in stage 2 of the assay.



Fig. 1.3: The tube format to be used as the site of the sample processing.

## 1.2 Aim

This work aims to develop and integrate into the Gene-Plex Robot Platform the hardware necessary for carrying out the described chemical processes, the required magnetic manipulations and the controller necessary to maintain the stipulated constant 60°C temperature.

## 1.3 Scope

The features required by the Gene-Plex Extractor, over those already part of the Gene-Plex Processor, can be grouped into 3 overall categories. These are detailed below, including a clear definition of their inclusion or exclusion from the scope of this work.

### 1.3.1 Mechanical

The summary of the extraction process to be implemented, given in Section 1.1.1, revealed a number of missing mechanical components when compared to the description of the Gene-Plex Processor given in Section 1.1.

**SBS Processing Module** As was noted in Section 1.1.1, the extraction process is to take place within cassettes consisting of 6 tubes. These must be located in the 3 SBS deck locations as marked in Figure 1.2, with each SBS location accepting 8 cassettes. The design of the module which will accept these cassettes is within the scope of this thesis and will form a large component of the design work undertaken.

**Heating Element** In order to create a commercially viable product, it has been stipulated that the tubes within each cassette where the lysis buffers and elu-

tion buffers are held (tubes 2 and 3), a temperature of 60°C must be maintained for the duration of processing. This is a core requirement of the extraction process and is included in the scope of this project.

**Magnetic Separation** The Gene-Plex Extractor can be seen to require magnetic manipulation of the silica beads in two different locations. In order to allow the extracted DNA or RNA to be captured after separation from the beads in tube 4, the beads must be retained in the tube while the liquid is aspirated by the pipette. Secondly, the magnetic beads must be captured within the pipette tip during the expulsion of the waste supernatant after all wash steps are completed. The conceptual design of the hardware for magnetic separation required in the process of tube 4 bead retention is defined to be within the scope of this work. The capture of beads in the pipette tip however, is not. The scope of this portion of work is limited to conceptual design due to AusDiagnostics' recent push for ISO certification. Due to these efforts, the validation and verification process of this component must meet a large number of requirements and must use input from a range of AusDiagnostics experts. Therefore, validation and verification is not within the scope of this work.

**Waste Disposal** Following the wash steps and the subsequent separation of the magnetic beads and the bound DNA or RNA from the wash buffer, the supernatant must be hygienically disposed of. This waste disposal method is required in order to ensure that no contamination occurs between the clinical samples being processed. It is also crucial to ensure that no contact can occur between the operator and the biological matter which is a by product of the extraction process. Due to the de-

mands of ISO certification process involving the handling of biological materials, this portion of work is excluded from the scope of this work.

### 1.3.2 Electronic

In order to account for the newly integrated capabilities of the Gene-Plex Extractor, some modifications to the Gene-Plex Processor electronics are required. Due to the temperature control requirements of the extraction process, an electronics board capable of communicating with the robot software and driving the heating elements appropriately is required. This however is not included in the scope of this work for a number of reasons. One of the components of the Gene-Plex processor is a device called the MTX Cycler. This device controls the temperature of the already extracted sample (during stage 2, amplification) precisely between set temperatures to enable PCR (Polymerase Chain Reaction) to occur and hence amplify the sample. The MTX Cycler controls the temperature of liquid volumes significantly smaller than those involved in extraction and in a different form factor, making it unsuitable for this application. It does however provide the necessary electronics and interfaces required to drive any standard form of heating element used here. Furthermore, the electronic board used to control the MTX Cycler is currently being integrated into a newly developed control board for the Gene-Plex Platform by AusDiagnostics engineers. This new board will also be capable of driving the heating elements selected for this application. Therefore, due to the redundancy of work on this component of the Gene-Plex Extractor and due to a suitable requirement existing, the development of the required electronic is not within the scope of this work.

### 1.3.3 Software

In order to enable the Gene-Plex Platforms controlling software to utilize the newly integrated capabilities, two main components of software must be created:

**Temperature Controller** In order to control the heating elements to maintain a stable and accurate 60°C for the lysis and elution stages, a temperature controller must be implemented. This temperature controller must be designed according to the temperature response of the heated hardware using appropriate methods and implemented as a controller in software. This element of the Gene-Plex Extractor's requirements will also form a core part of this work and is included within the project scope.

**Routine Addition** As was briefly noted in Section 1.1, the Gene-Plex Platform is highly adaptable in its ability to perform assays requiring differing liquid handling operations. The platform achieves this by utilizing a number of library routines which may be called upon the assay requiring a particular movement, such as expelling liquid, moving to a certain robot position etc. While the vast majority of these library routines will be directly effective within the Gene-Plex Extractor, due to the newly integrated capabilities, further routines will be required. These will include routines for the mixing of liquids in the cassette tubes, magnetic separation and a table of definitions which specifies the locations of each of the tubes and pieces of deck hardware. These software additions are not included within the scope of this work and will be implemented by software engineers at AusDiagnostics.

# **Chapter 2**

## **Literature Review**

### **2.1 Heating**

The thermal requirements for the extractor to be developed, as outlined in Chapter 1, are very similar in nature to those of a Polymerase Chain reaction (PCR) Thermal Cycling Device, albeit with simplified operations. The requirements of a PCR thermal cycler are driven by the need to cycle the temperature of an array of tubes containing a small volume of sample liquid through temperatures of 55°C, 72°C, followed by 92°C [1]. Due to the process involving upwards of 20 cycles between these temperature set points, ramp times for these changes in steady state must also be minimised to ensure the total processing time is commercially viable. The thermal requirements of the Gene-Plex Extractor are highly matched, with two exceptions. In this application the temperature of the sample liquid shall be held at a constant 60°C, as determined by research conducted by AusDiagnostics, as opposed to the multiple temperatures of a PCR cycler. Secondly, the cool down ramp rates for a PCR cycler are of equal importance to its ramp rates during heating, in order to achieve temperatures lower than the current

steady state in adequate times [2] [3]. In the application of the Gene-Plex Extractor, there is no need to pay attention to cooling ramp rates as the system will only cool at the completion of its operation. Due to the similarities evident between these two applications, a great deal of information may be gathered from PCR cycler design.

In order to generate the heat necessary to reach the required sample temperature, some form of thermal pump is required. A Thermoelectric Cooler (TEC), also known as a Peltier, is often used for liquid sample thermal cycling [4] among its' many other applications. A TEC is a solid state heat pump, controlled by the directional application of electric current across it's two terminals [5]. The direction of the applied current determines the direction of heat pumping across the module [5]. TEC's are constructed of pellets of n-type and p-type bismuth telluride semiconductors, connected in an alternating series [6]. The connections, made of copper, are bound to a substrate of ceramic alumina. This substrate forms the surface by which the heat generated is transferred. Figure 2.1 displays the arrangement of a TEC in a general case application. The TEC has shown through the reviewed literature to be common in PCR thermal cycler applications due to the above mentioned ability to pump heat in either direction, allowing ramping of temperature to be precisely controlled equally in both directions.

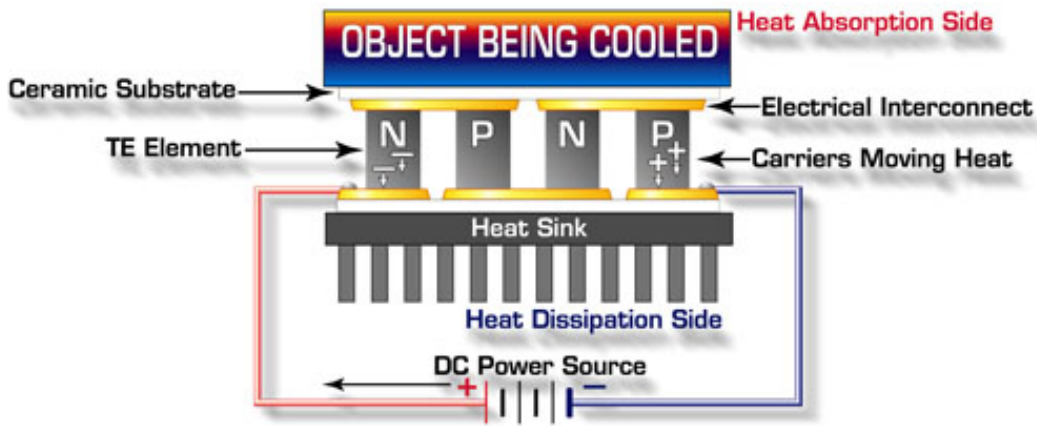


Fig. 2.1: Thermoelectric module as assembled in a typical application. [7]

When used in control applications, a TEC has the advantage of being able to not only add but to also remove heat energy as is required by the controller to achieve the desired response. Despite the TEC's ability to actively remove heat from a component, other active temperature removal methods may also be implemented. A passive approach to heat removal is that employed by a heat sink, or any simple surface area [8] [9]. This differs from an active approach, where airflow over the heat sink surface area is controlled via a fan, for example [8]. Such methods may be substituted for the directional heat pumping capabilities of the TEC, in order to achieve a similar level of temperature control. This leads to simpler possible options for heat pump selection, namely electric resistive heaters. Despite no reviewed literature describing these devices as the main heat source in thermal control for PCR in particular, they have been demonstrated to provide a crucial supporting role by Williams et al. The thermal cycler described in the work of Williams utilizes resistive heat strips to control the temperature of a sealing lid, preventing sample evaporation at the upper operating temperatures of a PCR thermal cycler [10]. While the application noted here

differs from the intended application within the extractor, where the device will be the primary source of heat, it demonstrates the feasibility of driving component temperature to a steady state value and hence represents a design possibility.

## 2.2 Cooling

In order to be able to control the temperature of the liquid sample as required, a method of evacuating heat must be present. A passive method alone, such as a heat sink in isolation, will not allow the process controller to drive a reduction in heat beyond the limits of conduction to the surrounding air [9] and as such performance will not be satisfactory. Along with heat dissipation being essential for control, the TEC elements have a maximum temperature differential of which they are capable of generating across their surfaces. This imposes the following constraint on the thermal system:

$$T_{hot} - T_{cold} \leq dT_{max} \quad (2.1)$$

This has been noted as highly significant in PCR cycler design [5], where one end of the TEC must be kept at ambient temperature to enable the maximum steady state value of 92°C to be reached safely. It should be noted that due to the maximum steady state temperature in this application being limited to 60°C and assuming a reasonable TEC differential limit,  $dT_{max}$ , this constraint is not critical. However, a TEC becomes less efficient as its temperature differential is increased [11]. As such, a method of heat evacuation must be present.

## 2.3 Controllability

In order to create a thermal system which is controllable within the context of stability and speed of response, attention must be paid to the thermodynamics of the device. Due to manufacturing constraints and standards, the tube which contains the sample itself is not optimal. A wall thickness of 1mm results in poor heat transfer characteristics from the heated block to the sample [12]. Another source of poor dynamics is any regions of mechanical connection between the heated block and external components [10]. Recommendations from the reviewed literature included the use of gasket material to limit thermal material between any surface contacts (Williams et al specifically recommends the use of ethylene propylene), along with the use of a groove extending through the majority of the thickness and hence limiting heat transfer to the mechanical connections [13] [11]. Mechanical connections are however only one cause of significant thermal gradient within the device. Care must be taken to reduce the severity and frequency of the occurrence of these gradients to maintain stability and performance in temperature response. After heat pumping has ceased, a temperature gradient will persist for a period of time that is proportional to the square of the distance between the hot and cold locations [10]. This has important implications for the number of sample tubes that may be heated within a single block. If the size of the sample array to be heated is too large, difficulty will be encountered achieving a uniform and stable steady state temperature [10]. Widomski et al note that despite efforts to reduce heat loss and hence gradients around the system boundaries via methods such as insulation, the

region of location of the heat source will continue to maintain a higher temperature. To counter this, it is suggested to use a rod of material with lower thermal conductivity (such as stainless steel within an aluminium block) to reduce the heat retained in this volume [11].

A number of measures may also be taken directly related to the heated block itself to ensure optimal thermal response. The concepts of static local balance and static local symmetry may be applied to obtain desirable heat transfer within the medium [10]. A state of static local balance refers to a state of constant temperature where all heat sinks are equalled by heat sources in a local area [10]. This essentially describes a state of thermal equilibrium, where the following condition is satisfied:

$$Q_{in} = Q_{out} \quad (2.2)$$

To ensure this balance is obtained, a device design should not incorporate overly effective heat sinks, without a proportional increase in the heat source capacity, and visa versa. The condition of static local symmetry requires that for a constant temperature and within a local region, the center of mass of the heat source is coincident to the center of mass of the heat sink [10]. Satisfying this condition will ensure that a constant, steady state temperature is achievable, without the presence of a permanent temperature gradient between the two centers of mass. The selection of heated block material along with manufacturing methods may also act to improve transfer properties. Aluminium 6061 is recommended due to its purity [10], which aids in even heat transfer [14]. It is further recommended that the heated block be manufactured via machining, due to the homogeneous structure

that results. This is beneficial in reducing any temperature gradients that may occur within the heated element due to mechanically or otherwise joined components or impurities or inconstancies that exist as a result of other manufacturing methods such as casting.

## 2.4 Temperature Sensors

The literature reviewed has presented various differing selections of temperature sensing technologies, the most prominent of which have been thermocouples and thermistors. Despite the overlapping application, the specifications of the two technologies are significantly different. The thermocouple has a large temperature range, with measurements capable of ranging from -270°C to 1800°C compared to the limited range of thermistors of usually around -90°C to 130°C [15] [3] [16]. The thermocouple and thermistor possess similar response rates along with similar accuracy, however due to the wider resistance range available, thermistors are able to achieve a high measurement resolution [15] [3] [16]. The two significant differences between the technologies are power supply requirements and linearity. Due to the welding of differing metal conductors at the measuring point, the thermoelectric effect results in a temperature dependant voltage being generated across the thermocouple terminals [15] [16] [3]. While this means the sensor does not require a power supply, it can introduce complications requiring a reference/compensating wire. Furthermore, changes to the conductor materials such as corrosion require that the sensor be calibrated on a regular basis, often as frequently as 3 months [15] [3] [16]. Thermistors use semi-conductive material that changes resistance with temperature. As such, measuring the temperature requires a current is passed through the

device [15] [3]. While the output voltage of thermocouples changes linearly with temperature, this is not true of thermistors. Hence, the output signal requires linearisation before it may be of use [3]. In commercial applications, thermistor technology is often also preferred due to its cost effectiveness [16]. While Resistive Thermal Detectors (RTD's) and Integrated Temperature Sensors appeared in a number of reviewed sources, they are not considered in depth due to the high level of signal conditioning required [16] [15] and the lack of observed uses in relevant thermal control applications.

## 2.5 Temperature Sensing

To utilize the thermal system to control the liquid sample temperature accurately, a method of obtaining a feedback signal is required. Complications exist however, due to the constraint that the sample temperature itself cannot be directly measured. Due to the thermal transfer characteristics discussed above, the placement of the sensing device is critical to the stability of the controlled substance [13]. Vilchiz et al studied the issues of sensor hardware placement and provided numerous recommendations to increase baseline stability. Using experimental methods, it was verified that the following one-dimensional heat equation holds:

$$s = \frac{L}{a} \quad (2.3)$$

Where  $s$  is the time taken for energy to flow from location A to location B,  $L$  is the distance between the two locations, and  $a$  is the thermal diffusivity of the material. This is relevant as it allows the time lag between a

controlled heating action at the heat source to the arrival of the generated heat at the location of interest to be determined. The experiment conducted tested two temperature sensing cases. One sensor was placed within the center of mass of the heated block, while the other was located as close as was possible to the heat source. The results obtained found that “there is a general advantage of control via sensing close to the heater, whether by temperature measurement, or by heat-flow control sensing.” [13]. Equation 2.3 is accountable for this result. When the sensor is placed at a greater distance to the heat source, the control effort is determined using a measurement that is not yet equalised due to the more severe temperature gradient. This error in feedback signal is reduced by the recommended placement strategy, such that “the reduction in the magnitude of the heater-induced oscillations achieved by this control strategy is at least one order of magnitude better than that of the temperature control at the core” [13].

A number of aspects of the experiments and findings the work of Wilchiz et al should however be considered. The sensing device used to make the presented conclusions were thermocouples, one of many sensing devices available. Despite the variances in accuracy and stability of measurements that are expected between differing sensing technologies, the results can be assumed independent of any associated error. Any error as a result of sensor output stability is of an insignificant order to magnitude of time when compared to the 1.07 min thermal lag situation generated by the experiment. Furthermore, one would expect a sensor technology of differing accuracy to produce a controlled output different to the desired reference input. This error is however not influential to the results given, which are concerned exclusively with the stability of the controlled response. The focus of the

experiment was the application of thermocouple technology in Tian-Calvet microcalorimeter devices. This does not detract from the relevance of the reviewed work for a number of reasons. The motivation for the study was to improve baseline stability in temperature control, via the application of improved temperature measurement strategies; a general outcome that is relevant to the work of this thesis. Further to this, the scale of the experiment conducted closely resembles the device to be developed, with the distance between sensor locations set equal to 3.5cm. Therefore, despite the differing applications of the work conducted, the recommendations and strategies found may be concluded as directly applicable.

## 2.6 Controller Design

With the necessary hardware in place and optimally set up, as has been discussed above, controller design and theory may be considered. The large majority of the reviewed literature, along with the instruments currently employed by AusDiagnostics, recommend or employ the Proportional Integral Derivative (PID) controller. As summarised by Vilchiz et al, “Although other types of controllers are also feasible, e.g., those based on fuzzy logic or artificial neural networks, the simplicity, good response, and low cost of PID-based control loops have motivated their popularity in industrial applications” [13] [5]. Despite the common application of the PID controller in thermal control applications, if a TEC is the selected source of heat, complications are presented. Due to the non-linearity of the device, PID coefficient selection involves the process of trial and error [5]. The strategies for PID design given were however applied to the thermal cycling requirements of PCR. This requires that 3 separate temperature controllers be implemented

for each of the temperature set points, to ensure the required performance is met equally at each [5]. While the characteristics of the PID controller are not effected by this difference, it does significantly increase the complications of coefficient selection in comparision to the application in the Gene-Plex Extractor. Further to the controller to be implemented itself, a number of sources give recommendations regarding relevant hardware. Cellatoglu et al investigated the dynamic performance of a process control system, with a focus on temperature controllers. The findings reveal that the word length of the ADC utilised is an important factor in reducing output error. A case study was conducted to assess the impact of increased word length on error, with results suggesting that 8 bits is the optimal value [17]. It was further found that an increase in word length beyond this point yields no reduction in error. The analysis conducted was however completed as a simulation, with no experimental verification evident. The electronic hardware implemented in other sources, such as the work of Shirafkan et al, differs from this recommendation. While not providing evidence to suggest the 8-bit recommendation is problematic, the successfully implemented controller utilized a 24-bit ADC.

## 2.7 Magnetic Separation

To ensure the target DNA is extracted as required, the device must include a robust means of capturing the magnetic beads. Despite offering an alternative means of magnetic bead manipulation, electromagnets are not investigated for application in the thesis due to a high level of complexity that is not required for this static, constant force implementation. Therefore, the re-

view of literature focuses on permanent magnets. While there are numerous compositions of magnets available, the rare earth variety and in particular the Neodymium composition (ND-Fe-B) are most suitable. Neodymium magnets offer the strongest solution, with an energy product of up to 56 MGOe [18]. Good mechanical characteristics and energy to size ratio make them suitable for fastening within a manufactured product, without undue difficulty. Importantly, given the requirement to capture beads within the heated block element, Neodymium magnets are stable in temperatures near ambient. Progressive loss of magnetism occurs at temperatures greater than 80°C [18], providing a 20°C margin of safety between the operating temperature of 60°C. This composition also holds a very high coercive force [18], allowing it to resist demagnetisation in the presence of external magnetic fields that will be present within the Gene-Plex Extractor, as a result of other hardware. Despite the specification of the superparamagnetic silica beads being a constraint determined by completed research at AusDiagnostics, a number of characteristics should be noted in order to obtain reliable bead capture capabilities. Shevkoplyas et al describes the force acting on a superparamagnetic bead due to an applied force. The context of this paper is the motion prescribed by the beads within a microfluidic chamber, however the general characteristics of the interaction between the beads and magnetic field are applicable to the capture required here. In order to saturate a suspension of superparamagnetic beads, an external magnetic field greater than 0.5T must be applied [19]. Saturation is the state where all beads' magnetic poles are aligned. In a state of saturation, the magnetic beads behave simply as permanent magnets [19] [20]. In order to ensure the complete separation of the magnetic bead dispersion within the sample liquid, this condition must be achieved.

The literature reviewed has allowed a number of critical elements of thermal control and magnetic separation, being the main requirements of the extraction system, to be recognised and evaluated within the context of this thesis. The similarity between the processes demanded by the extraction technique and the works discussed allow the information gathered to be applied directly to the benefit of the developed instrument. Those works which were an exception to this allowed general strategies and design characteristics to be collected, which may be applied with consideration in future development.

# **Chapter 3**

## **Methodology**

With the scope of the work now defined, the manner in which the required results will be obtained can now be detailed. The necessary additions as defined in Section 1.3, Scope, may will be implemented in the form of two independent assemblies in order to meet the requirements of the work. These two assemblies will be referred to as the Processor Module and the Magnetic Separation Station. The former will be the site of the chemical reactions as described in Section 1.1.1, The Extraction Process, and will be the hardware element that forms the SBS block on the Gene-Plex Extractor deck. Therefore, given it will house the full set of reactions, it will also encompass the software and hardware requirements of the liquid temperature control (including the associated controller), along with the magnetic separation required in tube number 4 of the cassette. The Magnetic Separation Station will be the location of disposal of the supernatant and therefore shall include the magnetic hardware required to physically manipulate the magnetic silica beads in order to retain them in the pipette tip while the waste is expelled. Given the biological nature of the liquid waste involved, this station will also include provisions for hygienically disposing of and storing

this waste.

## **3.1 Processor Module**

### **3.1.1 Hardware**

The hardware component of the Processor Module design is concerned with ensuring the module accepts the required cassette tubes, fits within the stipulated SBS space and provides a stable platform for the required temperature control using the knowledge gained in Section 2.3, Controllability. The work in this section will also include the selection of an appropriate heat pumping device. In order to ensure the requirements of the hardware elements are met, the design process is applied as follows:

1. Generation of concepts related to thermally isolating the heated and non-heated regions of the block. This includes a focus on the manufacturability of the resulting components.
2. Investigation into and selection of an appropriate heating method.
3. Full CAD design of hardware including provisions to accommodate the required tubes.
4. Utilization of 3D printing to test the fit of the cassette tubes in the block design.
5. CFD simulation using Autodesk CFD Motion to verify the performance of the selected heating element and the thermal stability of the final design.

### 3.1.2 Temperature Controller

This work will result in the finalisation of a software temperature controller capable of meeting the liquid heating requirements of the chemical reaction as detailed in Section 1.1.1, The Extraction Process.

In order to enable controller design to be commenced, the first step will be to assemble the completed Processor Module. Due to the complex dynamics of the heat transfer between the heating device and the liquid, a mathematical modelling method is not used. Instead, the system will be identified via the step input response plant identification method. To obtain the required response data, sensors will be placed strategically on the Processor Module to monitor and record key temperatures:

- The temperature at the centre of the block will be recorded as this sensor data will be utilized as feedback for the controller to be implemented. This follows the recommendations given in Section 2 by Vilchiz et. al.
- The temperature of the heat sink will be plotted to monitor the temperature differential created across the module.
- The temperature of the heated region of the module will be taken on its outer surface to determine the success of the design in creating a component that responds to temperature control in a responsive and stable manner.
- The temperature of the liquid within the cassette tubes will be measured as the final output of the system. The ability of the controller to drive this temperature to the desired set point will determine the success of the design.

To utilize this data for experimental plant identification, an Arduino will be used as an interface between the sensor electronics and MATLAB. This will enable the real-time monitoring and plotting of the data along with storage and subsequent analysis through the Arduino's Analogue input ports.

With the hardware now setup, the Processor Module will then be excited by a step input. The input will be provided by the same controlling electronics used in the final Processor Module. As was detailed in Section 1.3, Scope, the companies MTX Cycler electronics driver board will be utilized. The software controlling this board will therefore be modified to provide a constant step input to the Processor Module. The step input will be applied and the response data logged until a steady state has been achieved.

This data will have been logged in the MATLAB workspace in real-time, during the experiment. Prior to analysis however, the data will be pre-processed to remove any unnecessary features. For example, the data will be zeroed so that the response data begins at time  $t = 0$  and so that the response begins at  $0^{\circ}\text{C}$ . This will remove any effects of the varying room temperature at which the experiment may occur and ease the fitting of curves to the collected data.

To complete the plant analysis process using the pre-processed data, the MATLAB PID Tuner tool will be used. This tool provides a GUI for specifying a set of response data, the step input provided. This information is then used to interactively fit an appropriate function to the plants response data. The tool offers a number of plant structures to allow the correct plant to be identified. These range from a simple "One Pole" plant to a discrete time

system.

As a result of this process, the transfer function which represents the plant of the Processor Module will be known. This plant will be in the continuous time domain and is represented by:

$$G_p(S)$$

Before utilizing the identified plant for controller design, it will be verified via simulation in Simulink. The validation will be conducted by providing the plant an identical step input, as was done experimentally. Subsequently, the response will be verified to match that obtained from experimental data. The Simulink layout used to conduct this simulated verification is shown below in Figure 3.1.

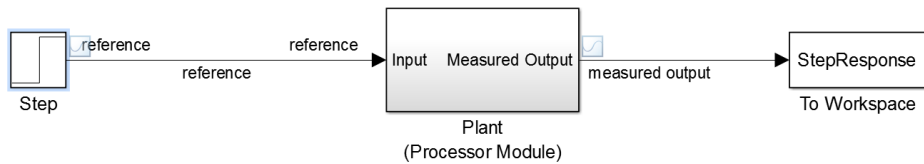


Fig. 3.1: The Simulink model layout used to validate via simulation the identified plant for the Processor Module.

With the transfer function representing the Processor Module now known, the process of controller design may be commenced. Two methods of controller design will be completed and implemented. Initially, a PID controller will be created. As was noted in Chapter 2, Literature Review, the most common method of control for thermal cycling devices in similar applications,

is PID control. This method is also able to be completed in short periods of time and therefore will allow the mechanical design of the Processor Module and heating element to be validated experimentally as early as possible. While this method is fast, there are however numerous advantages to the use of other methods. The second method chosen for this design process is the Direct Analytical Method (also known as Ragazzini's Method), in the discrete time domain. This method has been selected due the benefits of completing controller design in the z-domain with discrete time. By completing the design entirely in the z-domain, there is no need to convert the resulting controller from the s domain, allowing the controller to be directly implemented. By completing this second controller design, a greater degree of control is available in which the response of the system may be finely adjusted. The methodology used to form each controller is given below.

In order to create the PID controller, the MATLAB PID Tuner tool will be utilized. This tool will allow the identified plant to be taken directly from the plant identification step above and a controller tuned to suit the requirements. A system response time may be set along with the transient behaviour of the system. The tool then outputs the response of the system to the reference signal, as controlled by the PID controller. The tool then allows the following parameters to be inspected:

- Proportional gain,  $K_p$
- Integral gain,  $K_i$
- Derivative gain,  $K_d$
- Rise time

- Settling time
- Overshoot
- Peak response, as a percentage of the reference input
- Gain margin
- Phase Margin
- Closed loop stability of the system

With the outputs above provided, the tool allows for a time efficient method of designing a PID controller. This controller will then be directly implemented on the MTX Cycler software by directly substituting for the PID controller used in the previous application on the High-Plex Processor. This allows for immediate experimentation to be conducted.

The direct analytical method uses the principle that if the output that is required along with the input applied is known, the intermediate transfer function may be determined. This is represented by Equation 3.1, where  $C(z)$  is the required output,  $U(z)$  is the applied input and  $F(z)$  is the intermediate transfer function.

$$C(z) = F(z)U(z) \quad (3.1)$$

The method of feedback used for the controller is a unity feedback signal. Data provided by the utilized sensor will be processed to give a feedback signal with unity gain, to ensure any features of the raw signal are removed. For the unity feedback system picture in Figure 3.2,  $F(z)$  is given as [21]:

$$F(z) = \frac{G_c(z)G_p(z)}{1 + G_c(z)G_p(z)} \quad (3.2)$$

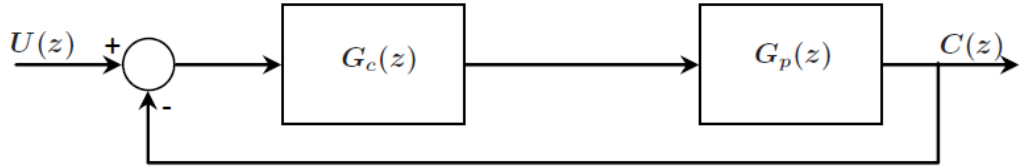


Fig. 3.2: The block diagram for a unity feedback system. [21]

Due to the plant identification completed earlier, the continuous time form of the system plant is known. Using MATLAB, this may be converted to a discrete time transfer function, with the appropriate sampling time selected. Therefore,  $G_p(z)$  is known.

Rearranging for the controller of interest,  $G_c(z)$  gives:

$$G_c(z) = \frac{F(z)}{G_p(z)[1 - F(z)]} \quad (3.3)$$

By equation 3.3, the direct method requires only that  $F(z)$  be determined to realise the controller. To complete the formation of  $F(z)$  and hence  $G_c(z)$ , the method below will be utilized. This method, as detailed by J. Katupitiya [21], provides a number of steps to ensure the resulting controller performs as required.

### Controller Performance

To define the response time of the controller, the pole locations are set. To do so, the desired time constant of the system,  $\tau$  is set and the s domain pole

is found by:

$$s = -\frac{1}{\tau} \quad (3.4)$$

This s domain pole is then transferred to the z domain via:

$$z = e^{sT} \quad (3.5)$$

Where T is the sample time of the controller. The resulting pole is then placed as a pole of  $F(z)$ .

It is also important to control the steady state error of the controller. To do this, the DC gain of the system is set to 1, resulting in the output equalling the input at a steady state. By setting the following, this can be achieved:

$$F(z)|_{z=1} = F(1) = 1 \quad (3.6)$$

### Pole Zero Cancellation

It must be ensured that a pole or zero cancellation does not occur in the unstable region of the Z-Plane, in order to ensure that this cancelled pole does not become a component of the formed characteristic equation. If a controller component cancels an unstable plant pole or zero in this scenario, it will influence the system so that it becomes unstable. These constraints will be dealt with via two stability constraints:

#### Stability Constraint 1

Stability constraint 1 addresses the instability that may occur if a pole of the plant  $G_p(z)$  is cancelled by a zero of  $G_c(z)$ . Firstly, all poles of  $G_c(z)$  are

tested for instability, where any pole  $z = p_0$  is unstable if :

$$|p_0| > 1 \quad (3.7)$$

If any pole is found to satisfy Equation 3.7, it is unstable and must be added as a zero of  $[1 - F(z)]$ . This addition removed the unstable pole and ensures the controller is not able to create the unstable cancellation.

### Stability Constraint 2

Stability Constraint 2 deals with the case that an unstable zero exists in the plant transfer function. Therefore, it prevents a pole of the controller from cancelling this zero in the unstable region. A zero of the controller  $G_c(z)$ , ( $z = z_0$ ) may be tested for instability by checking if it satisfies Equation 3.8:

$$|z_0| > 1 \quad (3.8)$$

Any zero satisfying this equation can be identified as unstable and dealt with by including it as a zero of  $F(z)$ .

### Causality Constraint

The causality constraint ensures that the designed controller is either proper or strictly proper. That is, that it only uses current or past terms in the calculation of controller effort and no futuristic terms. This is achieved by ensuring the pole-zero deficiency of the plant (i.e. its delay) is either the same as or less than that of  $F(z)$ . The pole-zero deficiency of the plant is the order of the denominator minus the order of the numerator, denoted as:

$$D[G_p(z)] = n \quad (3.9)$$

The pole zero deficiency of  $F(z)$  is given as:

$$D[F(z)] = m \quad (3.10)$$

If  $m = n$ , the controller is strictly proper. If  $m > n$ , the controller is proper. However, if  $m < n$ , then the controller is improper (will require futuristic terms) and the causality constraint is not satisfied. In this situation, the order of the denominator of  $F(z)$  must be increased until the controller is at least strictly proper.

### Controller Difference Function

Using the  $F(z)$  found using the previous steps, the controller transfer function,  $G_c(z)$  can then be calculated. This transfer function is converted into a function of the variable  $Z^{-1}$ , which is commonly known as the Digital Signal Processing (DSP) format. This allows the transfer function to be directly written as a difference function involving multiple error and controller effort terms with varying time delays. This difference function is the realised discrete controller.

### Simulated Validation

In order to validate the design of the controller prior to implementation, the design will be simulated via Simulink to validate its response to the desired reference input. The block diagram shown in Figure 3.3 will be used to conduct the validation and record the resulting data. The response recorded will be assessed against the controller requirements.

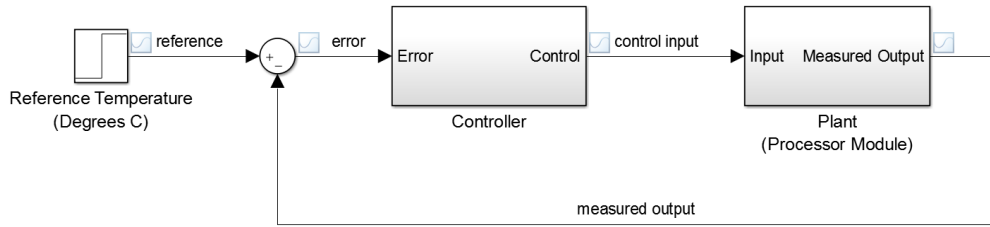


Fig. 3.3: The Simulink model layout used to validate via simulation the designed Processor Module controller.

Following the successful validation of the temperature controller, it will be implemented via software currently driving the MTX cycler, along with any required modifications.

### Experimental Verification

In order to verify the performance of the resulting controller, the following experimental verification will be conducted. The experiment will determine the ability of the controller to meet the steady state error, disturbance rejection, response time, overshoot and stability requirements when controlling temperature in the module. The method is as follows:

1. Assemble 4 complete Processor Modules
2. Using an Arduino as an interface and MATLAB as the data logger and analyser, measure the temperature in the tubes shown in Figure 3.4 for the duration of the experiment. This distribution will allow the performance at the extremes of the device to be determined.

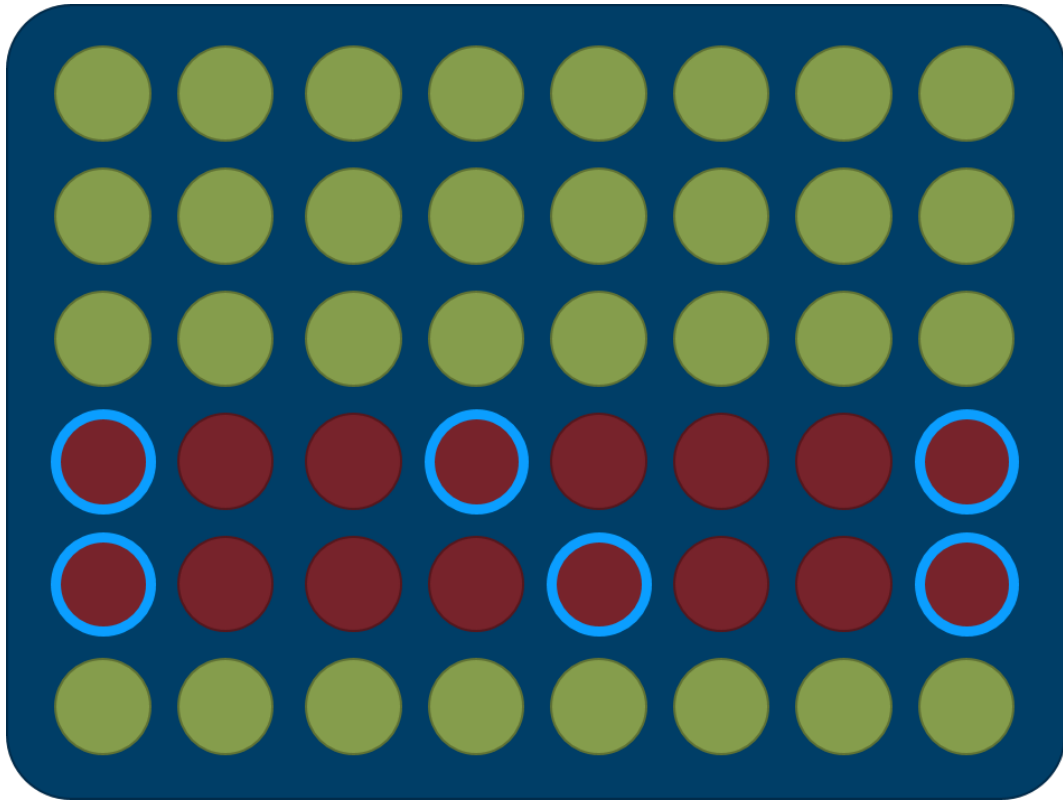


Fig. 3.4: Tube locations to be measured during temperature control verifications experiment. Non-Heated tubes are coloured green, heated tubes are coloured red, measured tubes are outlined in blue.

3. Begin data logging and live plotting.
4. Set the reference input to the controller to 60°C.
5. Collect data for a total of 30 minutes to capture the long term steady state performance of the module (to allow any slow heat transfers to be observed) along with the transient response.
6. Repeat the experiment for all four assembled modules. This allows for the controllers ability to reject disturbances caused by the differing of the plant properties to be determined as is caused by the slight differences in assembly.
7. Use the collected data to assess the consistency of the heating pro-

file and the temperature stabilisation across the tubes of the module. These results will be used to make conclusions regarding the designed controller along with the thermal characteristics of the hardware. It should be noted that the worst case response will be used to draw conclusions regarding performance to ensure all samples fall within the requirements.

### 3.1.3 Magnetic Separation

As the final stage of the extraction process is the removal of the clean sample from the waste beads, the success of extraction depends on the complete and reliable separation in tube number 4. To ensure this is achieved, the following design process and experimental verification is conducted:

1. An investigation shall be conducted into the various possible methods of magnetic separation in this application, taking into account the recommendations to use ND-Fe-B magnet compositions as found in the reviewed literature.
2. 3D Printed test jigs are created to test the effectiveness of the most suitable configurations via manual inspection.
3. With a preferred design selected, the test module is then 3D printed including the magnetic arrangement. This test module is assembled on the robot deck and verified experimentally via the method described below.

# **Chapter 4**

## **Results and Discussion**

The problem at hand along with the methodology employed to produce the solution are now well defined. Paired with an understanding of important previous works in this area and the technologies available, the design of each of the components may be given consideration. This chapter will present the designs of the required additions to the Gene-Plex Extractor, as were defined in Section 1.3, Scope. This will include relevant results from stages of the design process, the conducted simulations along with validations and verifications via experimental methods. Through the sections below, the reader will be familiar with the design of each of the components along with the resulting performance of the realised and implemented component.

## 4.1 Processor Module

### 4.1.1 Hardware

#### Thermal Isolation

The first consideration given to the design of the physical Processor Module was the thermal isolation of the heated and non-heated volumes. While there is no requirement stipulating that only tubes 2 and 3 may be heated, it was deemed thermally inefficient to heat the entire module. Such a design would also decrease the performance of the controller due to the larger mass to be heated. Therefore, the module was split into two regions, referred to as the Thermal Region and the Carrier. While the method of isolation needed to be effective to create a stable and controllable thermal system, a number of other design considerations were present:

**Manufacturability** The design of the thermal isolation method needed to consider the available manufacturing methods and their capabilities. For example, concept A shown in Figure 4.1, utilized a simple "trench" to create an air gap between the heated and non-heated regions of a single block of aluminium. While this concept satisfied the serviceability and cost objectives, there were a number of physical constraints preventing it from being feasible. Due to the geometry of the cassettes, the trench width was limited to 3mm across. At this size, the maximum depth at which the tooling could cut was stated to be 30mm [22]. At this depth, not only would a large area of material still connect the two regions, but the cost of machining would be high.

**Serviceability** When considering the serviceability of the product, two main aspects were key. This includes the initial assembly of the device after manu-

factory along with the periodic maintenance during its' operating life. The resulting design must ensure manual assembly is practical and that the replacement of components, such as sensors or heating hardware is considered.

**Cost** Given that a total of 3 Processor Modules are required for each Gene-Plex Extractor, the designs selected must be cost effective. While a number of high cost manufacturing methods or materials may have met the needs of the thermal isolation requirement, the cumulative cost required led to a need for alternative concepts to be generated.

With these factors in mind, four main concepts were generated with the goal of insulating the thermally controlled region of the Processor Module from the non-heated portion in mind. These concepts are displayed in Figure 4.1.

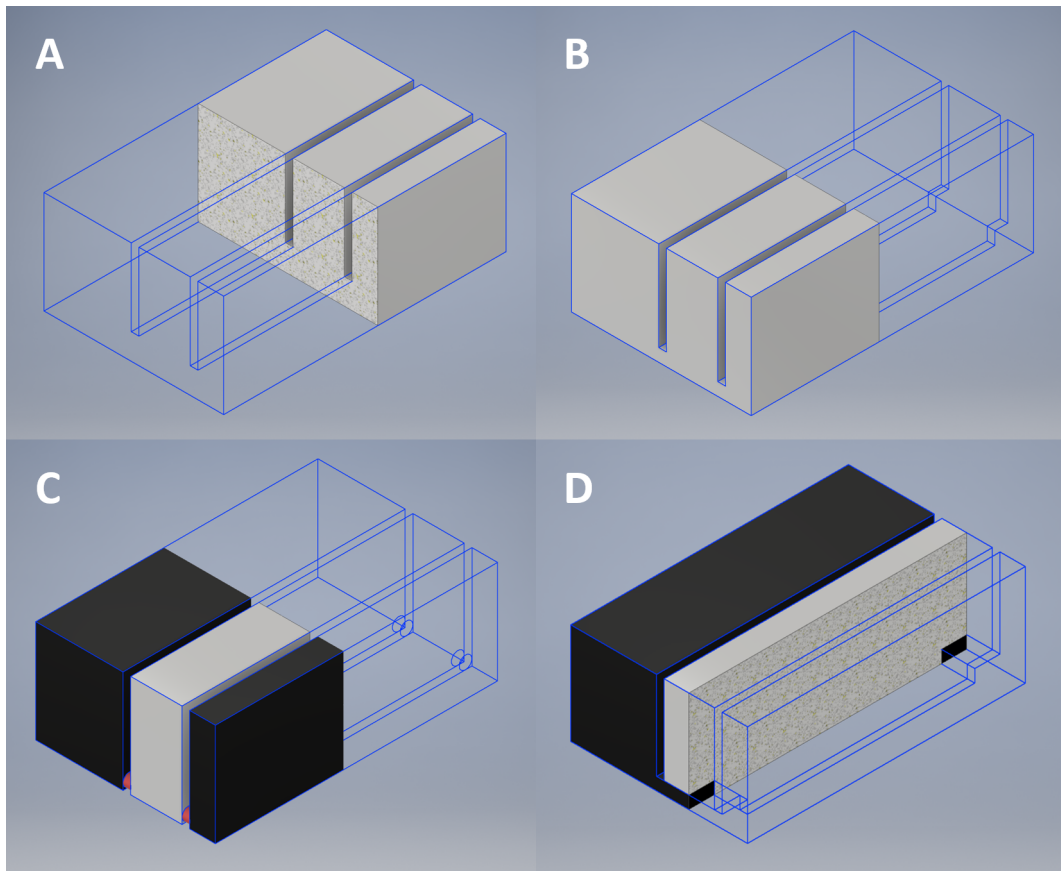


Fig. 4.1: CAD representations of the thermal insulation concepts.

Concept A features a groove machined into a solid billet of Aluminium, forming an air gap between the two regions. This concept has the advantage of simplicity, aiding with manufacture and serviceability. Its use of a single piece of material is also cost effective. It however had two main drawbacks. With the groove limited to a maximum of 3mm width and therefore 30mm deep, there is a large portion of material remaining which joins the two regions, leading to an undesirable level of heat transfer. Furthermore, the tooling costs involved with manufacturing this concept with the high aspect ratio groove are significantly higher than with traditional machining operations. For these reasons, this concept required further development.

Concept B furthered the ideal behind Concept A by improving on some of its flaws, namely the transfer of heat. This was achieved by including further machining operations on the bottom face of the block. Therefore, the groove depth could be through the thickness of the block, apart from the small connecting regions on the outer edges of each groove. This simple change allowed the connecting area of material to be reduced to only 10% of that of Concept A. Despite these improvements, the extra operations still require that small sections be machined at the same 30mm depth with the 3mm tool bit. Avoiding this is possible by performing machining operations on all four faces as opposed to only the top and bottom, however this will still carry added cost. Further to this, the homogeneous material and solid connection would allow for a more rapid heat transfer than was desirable. While aluminium is required for the Thermal Region due to its high level of heat transfer, this will result in large energy losses to the Carrier. It was therefore decided that the insulation should also make use of a thermally insulating material along with the physical separation used in the concepts to date.

Concept C moved in the direction of manufacturing the block from two separate materials and hence components. In Figure 4.1, Part C, the carrier is now seen to be of a different material, while the separating and insulating spacers are coloured in red. This allows the spacers to be manufactured from a highly insulating material, such as ethylene propylene as recommended by Williams et al. This concept provides excellent thermal insulation between the Thermal Region and the Carrier. The use of multiple parts however introduces another risk. The correct placement of the tubes in the Thermal Region is essential in ensuring the cassette tubes walls

contact the heated block and hence the liquid is heated as required. One of the purposes of the carrier is to ensure the tubes are correctly located and positioned. With the carrier now manufactured from two separate parts and the Region being separate again, the alignment of all three parts has a considerable degree of flexibility. Therefore, ensuring all components are properly aligned and the tube contact occurs depends heavily on the fastening used and the assembly process itself. While possible to design an assembly method and fastening system that would locate the three components accurately, it was decided that this should be a feature of the design itself.

Concept D addressed these issues by using a single piece Carrier manufactured from a thermally insulating material. This was then designed so that the aluminium Thermal Region would sit directly inside a space machined from it. The use of this space meant that tolerances could be used to directly control the alignment of the Carrier and the Thermal Region and hence create a reliable tube fit to ensure consistent heating. In order to control the variation among the manufactured parts, the tolerance was set as a locational clearance fit. This fit provides a tight fit for locating the two parts, however under no circumstances allows interference and hence allows easy assembly and disassembly for servicing [23]. The details of this fit are given in Table 4.1.

Fit Classification	Minimum Clearance	Maximum Clearance
Locational Clearance	0.1mm	0.2mm

Table 4.1: Details of Locational Clearance Fit.

Due to the high degree of positional accuracy achieved by the fit de-

scribed above, the design was able to be further simplified. Whether a TEC or resistive heaters were chosen, a heat sink was required on the bottom side of the device to fulfil the requirements of controller. This heat sink must be located on the bottom of the Thermal Region to extract thermal energy. Therefore, it may be used to "clamp" the single piece carrier and secure it in position. In this arrangement, the locational clearance fit locates the components in the X and Y directions, while the clamping force provided by securing the Thermal Region to the heat sink with the Carrier in between secures the Z direction movement. This allows a further reduction in hardware fasteners which not only increases manufacturability, but also reduces heat transfer due to conductive transfers that are created by fasteners such as bolts.

### **Heater Selection**

In order to achieve the heating requirements of the extraction process, two main heating devices were considered, as were explored in Chapter 2, Literature Review. These were the solid state TEC and the resistive heat strip.

After consideration of the properties of each device, the TEC was selected as the heating device to be used. While the resistive heating elements are cost effective, easily installed, possess a long service life and can generate large quantities of thermal energy, the TEC has a number of significant advantages. The TEC modules are a solid state device and hence provide a highly reliable means of thermal management. The devices, provided they are installed correctly, may last for up to 200,000 hours of use [24]. This figure is supplied by Ferrotec, the supplier of TEC's used by AusDiagnostics, and is stated to be an accepted industry standard MTBF (Mean Time Be-

tween Failures). Along with this high level of reliability, these modules are capable of providing precise temperature control to within  $\pm 0.1^{\circ}\text{C}$ . This advantage is paired with their simple power supply requirements, being able to be controlled via PWM (Pulse Width Modulation) directly from a DC power source. The TEC devices available are also capable of outputting significant amounts of thermal energy, with single state devices able to transfer up to  $6 \text{ W/cm}^2$  of device surface area [24]. By far the greatest advantage however, is the ability of the TEC to pump heat in either direction to enable both heating or cooling of the target component with the same installing. As was described in Chapter 2, Literature Review, this is controlled simply by inverting the direction in which current is applied to the terminals of the TEC. This has large significance for the control of the system temperature, as the controller can actively drive the temperature in the necessary direction to drive the error to 0, as opposed to relying purely on passive methods or even fan based cooling.

With the device to be used now selected, the power requirements of the TEC needed to be determined. In order to ensure the selected TEC would be capable of driving the temperature of the Thermal Region to  $60^{\circ}\text{C}$ , the thermal transfers of the system needed to be understood. As the Thermal Region reaches its' target temperature, losses will begin to occur at a greater rate to its surroundings due to the increasing temperature differential. The power of this energy transfer must be at the very least matched by the power output of the TEC to maintain a stable temperature, or exceeded to drive the temperature change at an acceptable rate. To determine these variables, a number of design parameters are required:

$T_h$  This is the maximum hot side temperature of the TEC module. For this application, the module will need to drive the Thermal Region to 60°C and therefore this temperature is selected. However, it is recommended that for large thermal loads, or those where the path of heat transfer is greater than 25mm, that this variable be increased by 5°C. This application involves both of these conditions and therefore:

$$T_h = 65^\circ\text{C}$$

$T_c$  This variable is determined by the minimum expected ambient temperature in which the device will work within the capacity of the applied heat sink. If the system operates with a small thermal load and adequate heat sinking, then the following equation is applied:

$$T_c = T_{ambient} - 5^\circ\text{C} \quad (4.1)$$

However, for a system with a large thermal load and a small level of heat sinking, the following is substituted:

$$T_c = T_{ambient} - 15^\circ\text{C} \quad (4.2)$$

With the device matching the conditions of a large thermal load with small heat sinking, Equation 4.2 is applied. Given that the Gene-Plex Extractor will operate within enclosed indoor facilities, 20°C was selected as the minimum expected ambient temperature. Therefore,

$$T_c = 20 - 15$$

$$T_c = 5^\circ C$$

In order to calculate the thermal load which the TEC's must displace to drive a temperature change, the various thermal transfers of the system must be estimated. These loads may be split into active and passive loads:

$$Q = Q_{active} + Q_{passive} \quad (4.3)$$

**Active** These loads are due to the power dissipated by the device as part of the electrical components. In the case of the Processor Module, this load is negligible due to the significant separation between the electronics and the thermally controlled elements:

$$Q_{active} = I^2 R = 0$$

**Passive** These loads are those due to heat transfers within the device and to its surroundings. These consist of radiation, convection and conduction:

$$Q_{passive} = Q_{radiation} + Q_{convection} + Q_{conduction} \quad (4.4)$$

Radiative thermal transfers are found using:

$$Q_{radiation} = F\epsilon\sigma A(T_h^4 - T_c^4) \quad (4.5)$$

where,

$F$  = Shape Factor = 1 (assume worst case scenario)

$\epsilon$  = Emissivity = 1 (assume worst case scenario)

$\sigma$  = Stefan-Boltzmann Constant =  $5.667 \times 10^{-8} W/m^2 K^4$

$A$  = Surface Area ( $m^2$ )

$T_h$  = Maximum TEC hot side temperature (K)

$T_c$  = Minimum TEC cold side temperature (K)

Convective thermal transfers are found using:

$$Q_{convection} = hA(T_h - T_c) \quad (4.6)$$

where,

$h$  = Convective heat transfer coefficient =  $21.7 \text{ W/m}^2 \text{ }^\circ\text{C}$

$\epsilon$  = Emmisivity = 1 (assume worst case scenario)

$\sigma$  = Stefan-Boltzman Constant =  $5.667 \times 10^{-8} \text{ W/m}^2 \text{ K}^4$

$A$  = Surface Area ( $m^2$ )

$T_h$  = Maximum TEC hot side temperature (K)

$T_c$  = Minimum TEC cold side temperature (K)

Conductive thermal transfers are found using:

$$Q_{conductive} = \frac{KW}{L}(T_h - T_c) \quad (4.7)$$

where,

$K$  = Thermal Conductivity of material ( $\text{W/m } ^\circ\text{C}$ )

$W$  = Cross sectional area of material ( $m^2$ )

$L$  = Length of thermal transfer path (m)

Using these equations, the thermal load of the Thermal Region was de-

terminated to be:

$$Q \approx 47W$$

This figure was determined using the equations discussed via a MATLAB script. For this estimation, some simplifications were made. This includes neglecting the effects of radiative loads due to their low weighting in this result. Furthermore, only the significant bodies and thermal transfers in the assembly were modelled. The purpose of obtaining this estimate was to guide a good starting point for TEC selection. Comprehensive CFD was completed as a later step, as detailed below, and therefore a high level of accuracy was not necessary in this calculation.

Using this figure and comparing the available TEC modules available from suppliers, it was decided that this power requirement could be most effectively met by utilizing 3 TEC's, each with a 16W capacity. This divide matches closely with the available module power outputs when considering the area to which they will be mounted, as achieving this output from a single device would result in a module that exceeds the area available for mounting.

The maximum temperature differential expected in this application is  $\Delta T = T_h - T_c = 60^\circ\text{C}$ . This is comfortably within the  $72^\circ\text{C}$   $\Delta T$  limit of a single stage TEC. Therefore, single-stage modules will be used.

The modules selected for use were the Ferrotec 9500-035-085 B. The device has dimensions 15.1mm (W)  $\times$  29.8mm (L)  $\times$  3.94mm (H). It's performance values are summarised in Table 4.2. This module can be seen to

exceed the thermal power requirement by a comfortable margin of 4 Watts.

I Max	V Max	$\Delta T$ Max	$Q_c$ Max
8.5 A	4.8 V	72 °C	22.0 W

Table 4.2: Ferrotec 9500-035-085 B Performance Specifications.

### CFD Simulation - Initial Design

With the TEC modules selected, the module's design was completed in Autodesk Inventor Professional to enable CFD Simulation to be completed. This first stage of CFD was used to gauge the first design iterations ability to heat the Thermal Region to the desired set temperature.

To ensure the efficient usage of computing resources, the design was simplified appropriately with the following changes made:

- Removal of all corner fillets and chamfers.
- Removal of interferences between components, such as where foam insulators will be compressed.
- Detailed TEC module component replaced with a simplified rectangular prism.
- Bolted connection and associated holes removed.
- Circuit board removed.

These simplifications allowed for the model to be meshed with a total of  $2.1 \times 10^6$  elements.

While the specifics of the CFD setup are not presented, it is noted that the Chimney approach was used for the boundary condition setup. This

setup is applied to the body of air surrounding the model. This body of air then has two boundary conditions applied. The first is a 25°C temperature boundary condition on the bottom face. This is then completed with two 0 kPa pressure boundary conditions on the top and bottom faces. With this setup, the simulation was run to convergence.

## Discussion

The simulation conducted provided a number of key results. These include the adequate performance of the TEC modules and setup selected, evidence to support reducing the number of TEC modules used in each Processor Module and finally, possible areas in which the mechanical design can be improved.

A study of the cross sectional temperature gradient throughout the Thermal Region displayed a high level of consistency across the component and therefore validated the mechanical design.

The simulation also demonstrated the TEC modules were operating at a very high Coefficient of Performance (COP). It should be noted that it is in fact possible to operate at COP's of greater than 1, as this value is obtained by the equation [25]:

$$COP = \frac{Q_h}{P_{in}} \quad (4.8)$$

where,

$$Q_h$$

is the thermal power generated by the TEC at the hot side.

$$P_{in}$$

is the power supplied to the TEC.

The COP obtained in this simulation suggests the TEC's are operating below their maximum operating point in order to drive the Thermal Region to this temperature. This was further shown by the maximum current value, which demonstrated the module operating at less than 10% of it's maximum, as was given in Table 4.2. While operating at a fraction of  $I_{max}$  gives a higher efficiency, there are advantages of operating at a point nearer this value. Due to the Ferrotec TEC modules costing around \$16.00 each, reducing the number of TEC's per Processor Module is advantageous, due to the cost reduction this would achieve for each Gene-Plex Extractor.

Finally, the results of this initial simulation identified an area through which significant heat transfer was occurring and must be reduced. This region was found to be at the meeting plane of the Thermal Region and the Carrier, where an overlap between the two parts was created along the entire perimeter of the Thermal Region. This design feature was used to ensure a level placement and proper location of the Thermal Region with respect to the Carrier. However, the area of material used to achieve this may be reduced significantly to avoid the thermal losses occurring as a result.

### CFD Simulation - Refined Design

The results drawn from the initial experiment were then applied to form a refined design. This section described the results obtained from the analysis of this design. The two major refinements made include the reduction of TEC modules from three to two, along with the reduction in contact area between the Thermal Region and the Carrier.

The refined design was then simulated using an identical setup as was used previously. The results of this simulation, after the solver had reached convergence, are given in Figure 4.2. Once again, the convergence plot for this simulation is provided in Appendix A.

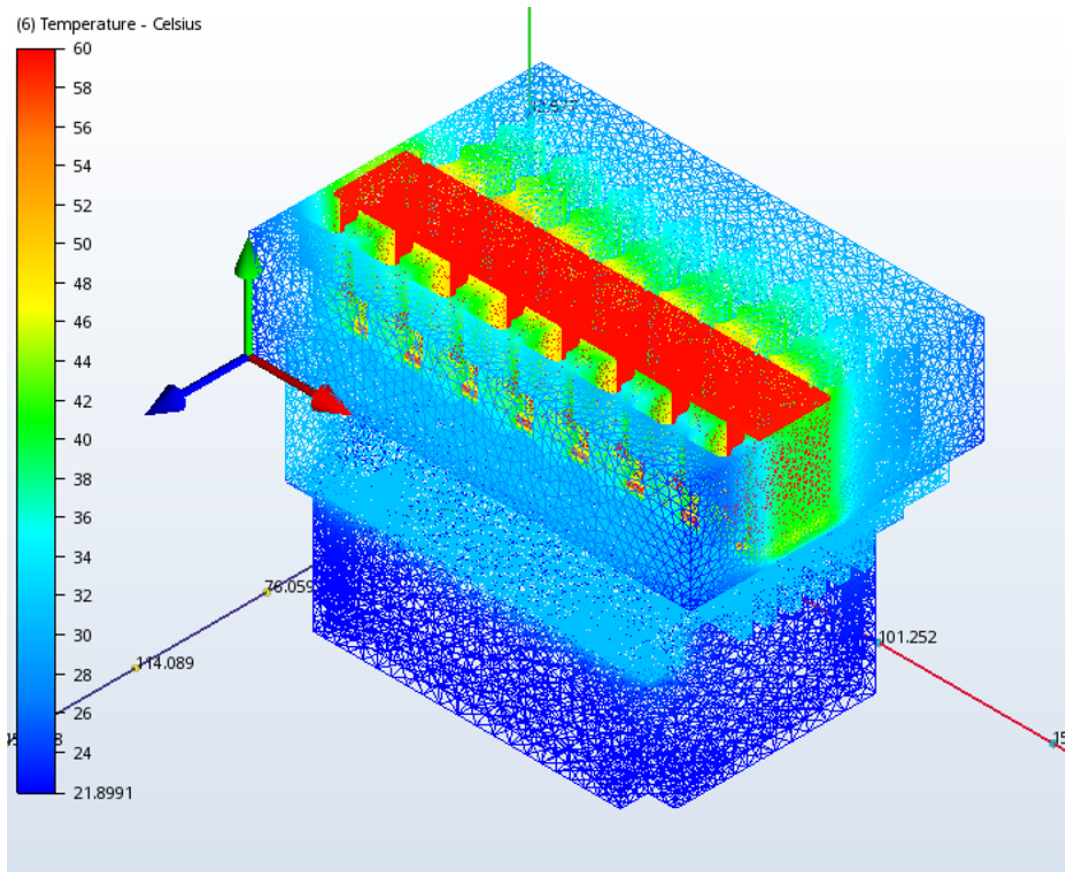


Fig. 4.2: Final results of the CFD Simulation of the refined design.

Figures 4.3 below show the temperature variation across the Thermal Region normal to the X, Y and Z axes.

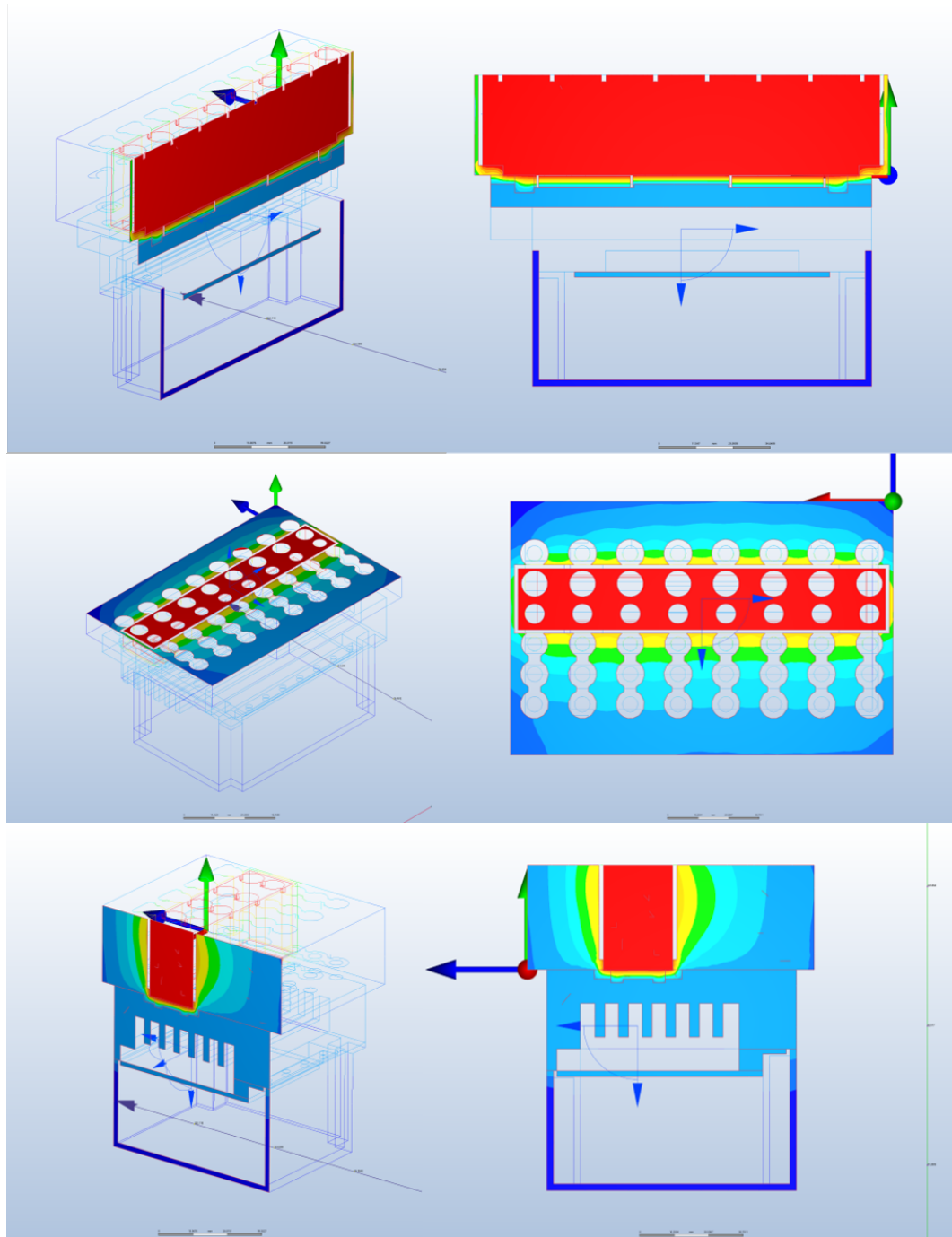


Fig. 4.3: Spatial variation of temperature through the XY, XZ and YZ planes of the Thermal Region.

The thermal transfer between the Thermal Region and the Carrier are shown along the YZ plane in Figure 4.4.

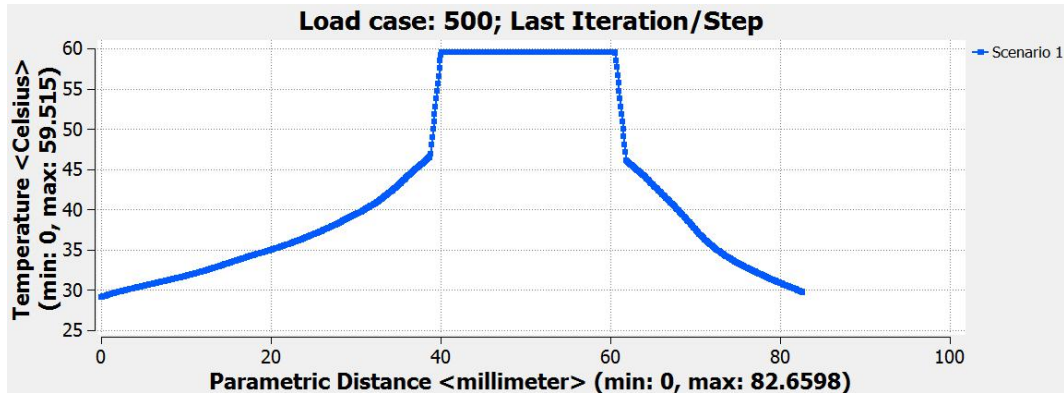


Fig. 4.4: Thermal Losses from Thermal Region to Carrier.

The critical TEC performance values are summarised below in Table 4.3:

TEC No.	1	2
Status A	Normal	Normal
Cold Side Temperature	31.00 °C	31.25 °C
Hot Side Temperature	60.00 °C	60.00 °C
Power Input	3.53 W	3.37 W
Operating Current	1.43 A	1.40 A
COP	0.92	0.94

Table 4.3: Ferrotec 9500-035-085 B Simulated Performance.

## Discussion

By comparison between the results obtained by simulating the refined design as opposed to the initial design and by analysing the critical data points, a number of key points may be noted.

Most critically, the sectioned views in Figures 4.3 show a consistent temperature distribution is still attained despite the drop to two TEC modules. The results show an average temperature across the Thermal Region of  $59.58^{\circ}\text{C}$ , and a minimum temperature of  $58.78^{\circ}\text{C}$ . The results validate the performance of the hardware design in providing a stable platform for temperature control to be carried out within.

Considering the performance figures of each of the TEC modules in Table 4.3, the suitability of the reduction in TEC units can be assessed. Given the minimum COP of 0.92 and the maximum operating current of 1.43 A resulting in a 16.8% usage of each devices operating limit, the modules are shown to be working within their operating limits at a high efficiency when holding the Thermal Region at a steady state  $60^{\circ}\text{C}$ .

As a result of the experiment conducted, the configuration simulated is seen to achieve the stipulated operating requirements as well as make effective use of the capabilities of the heating components. Therefore, this configuration is selected as the final design for the Processor Module.

### 4.1.2 Final Mechanical Design

With the mechanical design validated by a thorough CFD simulation and analysis, the final design was determined and finalised. The following is a summary of the notable features of the result of this process.

Due to the results of the intial simulations in Section 4.1.1 and the validation obtained in Section 4.1.1, the method of locating the Carrier on the

Thermal Region was revised. The result is the locating design displayed in Figure 4.5, where a small overlap of the Thermal Region on the Carrier is used to lock the Carrier between the Thermal Region and the heat sink it is fastened to. This design choice allows the Carrier to be held in place with no fasteners. As was discussed in Section 4.1.1, this will constrain only the movement in the Z direction. Therefore, the locational clearance fit of Concept D is used to ensure complete location of the Carrier, without the direct use of a fastener.

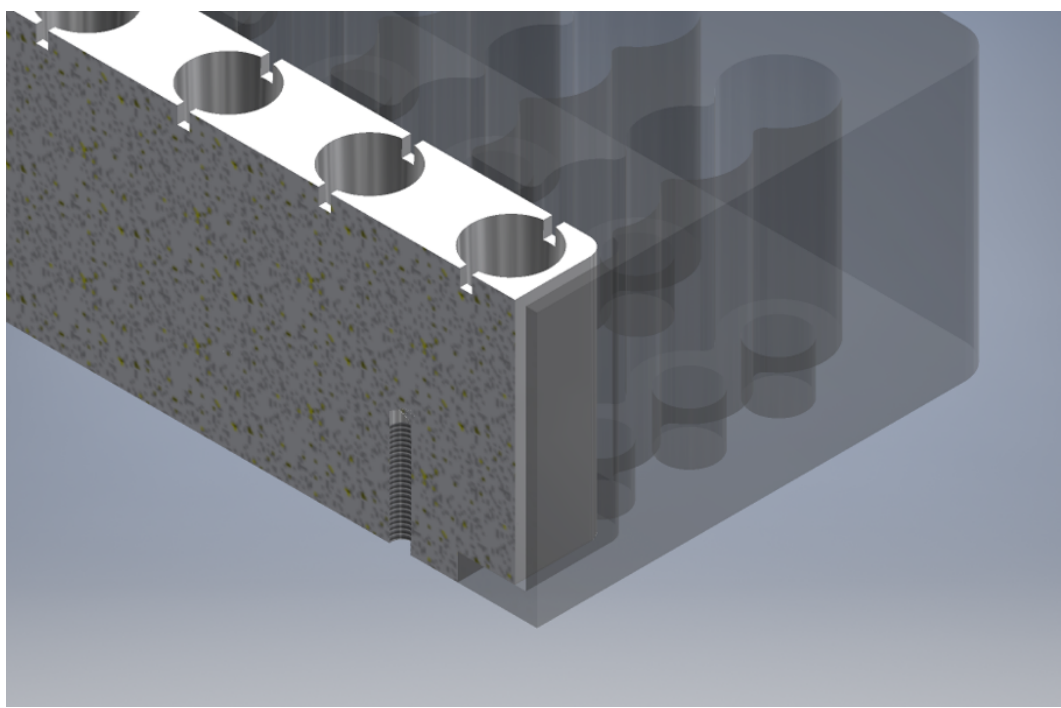


Fig. 4.5: Design for accurate carrier location around the Thermal Region.

The design of the Carrier itself was considered to ensure it fulfils two main purposes. These are prevention of user contact with the hot Thermal Region and ensuring the correct positioning of the cassette tubes in the Thermal Region. The first purpose is to ensure the design complies with Standard BS EN 61010-1:2010 [26] in preventing the user from unintention-

ally making contact with the hot component during normal operation. The combination of the Carrier and the installed cassette tubes provide full coverage of the Thermal Region and hence prevent such contact occurring unintentionally. Finally, the design of the Carrier is such that it does not allow the cassette tubes to be misplaced by the user. This is achieved via a number of design elements. Firstly, the Carrier itself prevents the cassette tubes from being positioned in the Processor Module in the reverse orientation. The fit of the cassette tubes in the Thermal Region is then controlled by the geometry of the tube holes in the Carrier wells. As is pictured in Figure 4.6, the cassette tubes are tightly fitted within the Thermal Region, while sitting in the Carrier supported only at their base to control their height. This ensures that the fit within the Thermal Region is accurate independent of the manner in which the user places the tubes into the Processor Module, by preventing rocking. Furthermore, it ensures any deviation of the Carrier's position around the Thermal Region due to the locational clearance fit does not force the cassette tubes out of contact with the heated material.

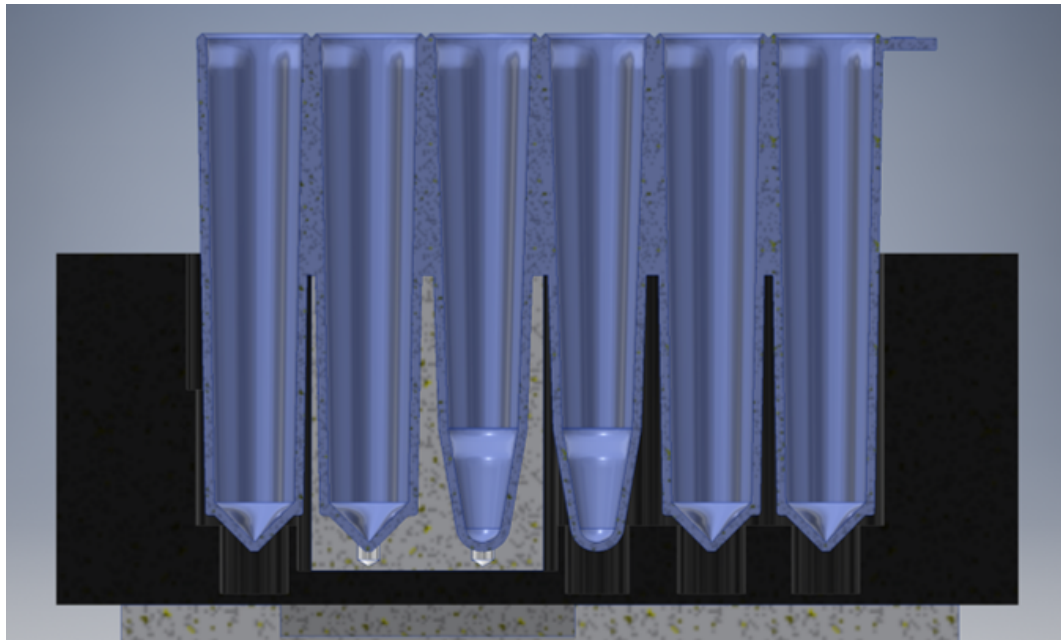


Fig. 4.6: Cassette tube fit within Carrier and Thermal Region ensures a reliable contact on the heated tubes.

The heat sink designed for the Processor Module is required to maintain the stable thermal state during both heating and steady state operation. As was noted in Chapter 2, Literature Review and in Section 4.1.1, the TEC modules will only pump heat if they are operating below a  $\Delta T$  of  $72^{\circ}\text{C}$ . the design parameter set was to maintain the heat sink at a maximum of  $15^{\circ}\text{C}$  below ambient. It was decided to achieve this via passive cooling of the heat sink using only natural transfers, as opposed to an active approach, for example using a fan. This was to reduce overall system complexity, system power requirements and cost of each Processor Module. Therefore, it was necessary to ensure the heat sink comprised of a large thermal mass and surface area to promote heat transfers with the surrounding air and to ensure a slow rate of response to the heat energy that the TEC modules will introduce.

Further to this, the heat sink is used as the mounting location for the  
October 24, 2016

TEC modules and the associated wires and sensors. The final design of the heat sink is pictured in Figure 4.7, with the two TEC's. The insulator and the TEC Spacers shown in grey and black respectively.

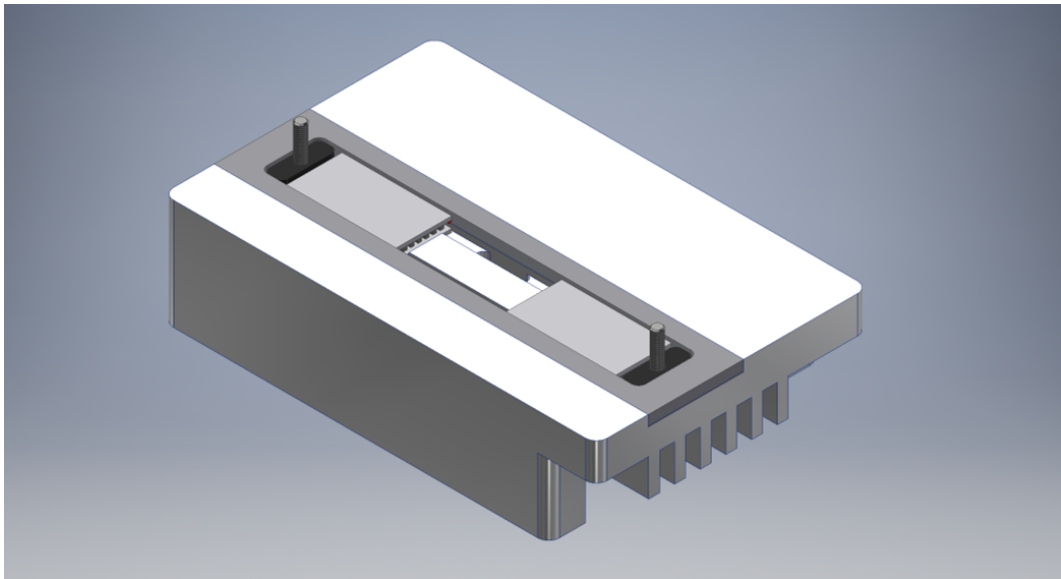


Fig. 4.7: The final heat sink design, including TEC housing and wire and sensor accommodation

The insulator placed around the perimeter of the TEC modules is a critical design feature. It ensures that the heated and cooled regions of the Thermal Region and heat sink respectively are not able to transfer heat energy via conduction to one another, and forms the separating piece between both components. The insulator is made of a silicon gasket insulator [27], and has been proven effective as an insulator in the AusDiagnostics MTX Cycler. Further to this, the silicon material used has a surface skin that results in a very low absorption of liquid [27]. This feature has allowed the insulator to form a seal around the open areas of the design, to ensure no spilt liquid or chemicals are able to enter the internal device area.

The TEC Spacers are two components placed around the bolted connections, shown in black. These components are included in order to ensure the operation life of the TEC modules is not compromised by uneven loading. Due to the asymmetrical design of the heat sink, it is possible that an uneven load may result across the face of the TEC modules. It is also critical that the modules are clamped between an evenly spaced void to reduce as much as is possible any shear loading. The Acetal TEC Spacers achieve this by ensuring the heat sink and Thermal Region are parallel when assembled, while also ensuring the spacing between the TEC surfaces is consistent. The components are machined from Acetall, due to its properties as a good insulator, good thermal stability and the high accuracy with which it may be machined.

In order to ensure the TEC modules are then adequately clamped and are in ideal conditions, the two fastening bolts must be torqued precisely. The recommendation provided by Ferrotec, the TEC manufacturer, is as follows:

$$\tau = \frac{S_a A}{N} Kd \quad (4.9)$$

where,

- $S_a$  is given as 25-50 psi for a cycling application, or 50-75 psi for static applications such as this.
- A is the total surface area of the TEC modules.
- N is the number of bolts used to clamp the modules.
- K is the torque coefficient, recommended as 0.2 for steel fasteners.
- d is the nominal bolt diameter. In this case, two M3 bolts are used and

hence  $d = 3$ .

Therefore:

$$\tau = \frac{(3444738pa)(9 \times 10^{-4}m^2)}{2}(0.2)(3 \times 10^{-3}m)$$

$$\tau = 0.93Nm$$

A fully exploded rendering of the final Processor Module design is given in Figure 4.8.

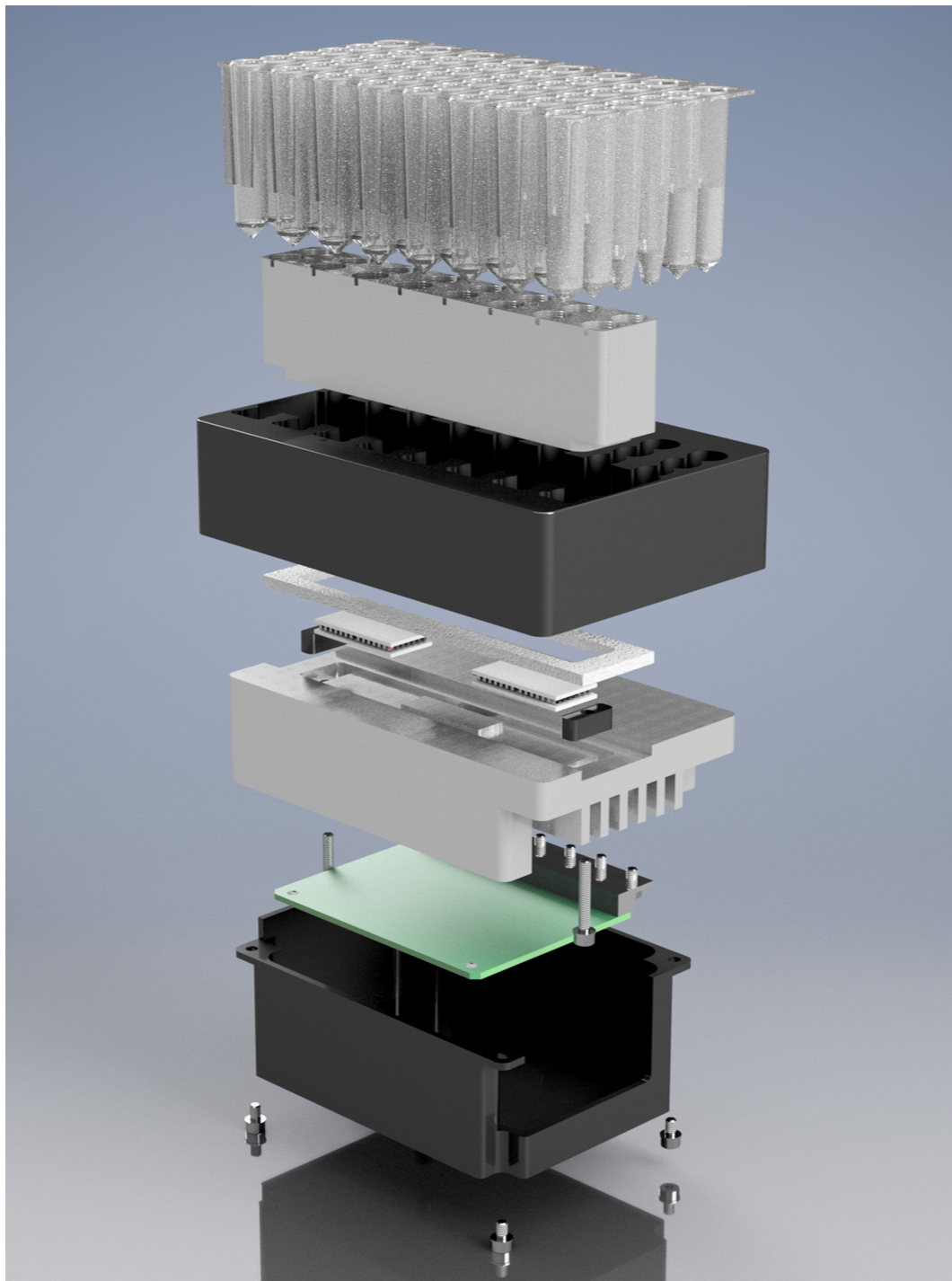


Fig. 4.8: An exploded representation of the final Processor Module Design.

### **4.1.3 Processor Module Assembly**

This section provides a brief and summarised overview of the assembly process of one of the 10 Processor Modules which were manufactured following

**October 24, 2016**

the design and validation completed. This work is completed in preparation for the controller design, detailed in Section 4.1.4. The full set of manufactured components are pictured in Figure 4.9, and includes (from left to right) the:

- Carrier
- Heat sink
- TEC Spacers
- Thermal Region
- Ferrotec TEC Modules
- TEC Gasket/Insulator

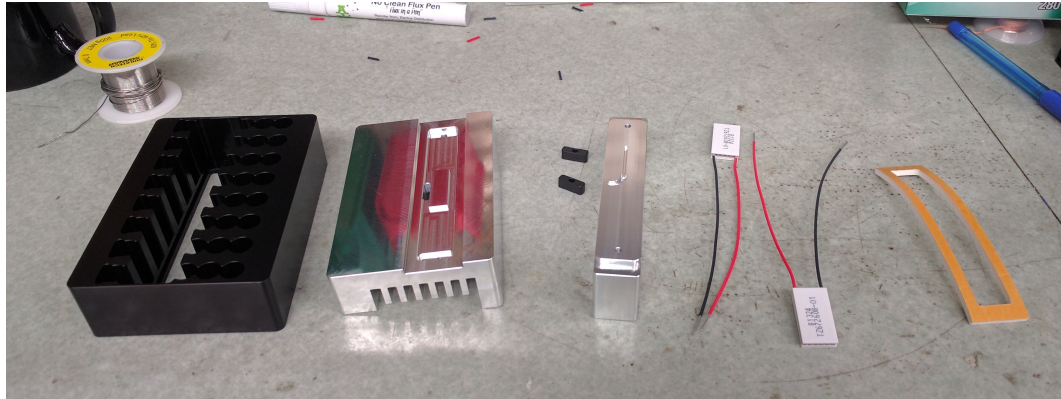


Fig. 4.9: All Processor Module components (MTX Cycler electronics board not included).

The first stage is to prepare the two TEC modules to be used within the assembly, as shown in Figure 4.10. This required wiring and soldering the modules in series and protecting the connections to ensure reliable operation.

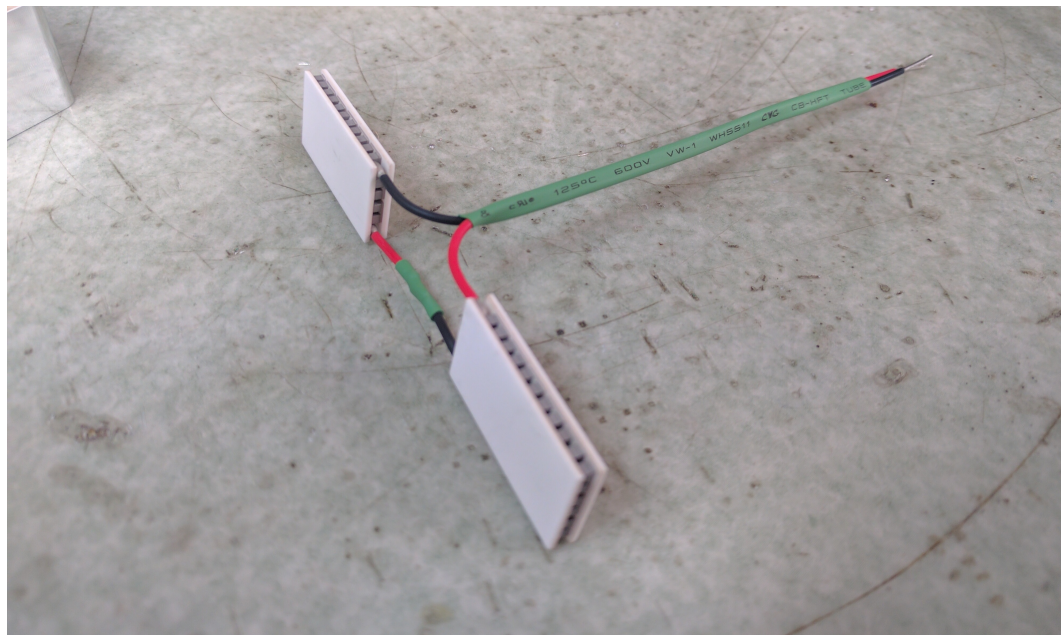


Fig. 4.10: The assembly of the Processor Module's two TEC modules.

Prior to placement in the heat sink, it is crucial that a thermally conductive paste is applied evenly to the surface as in Figure 4.11. The thickness of this coating must be 0.02mm or less, however ensures full contact is made between the TEC and the surface along with providing necessary lubrication for the expansion experienced by the device.



Fig. 4.11: Application of thermally conductive paste to the contact area of the TEC modules.

Following this, the TEC's may be placed into the heat sink and their wiring directed through the port. The TEC Spacers and the insulator/gasket is also attached via its adhesive backing to the heat sink. A final identical layer of thermal paste is once again required on the hot side of the TEC modules. This stage is shown in Figure 4.12.



Fig. 4.12: Placement of the TEC modules, gasket/insulator and TEC spacers into the heat sink.

Before final positioning, the required wiring is added to the thermistor sensor and protected, as shown in Figure 4.13.



Fig. 4.13: The thermistor sensor is prepared with additional wiring.

The thermistor sensor is then epoxied into the Thermal Region and encased in thermal paste to ensure accurate measurement. This step is pictured in Figure 4.14.

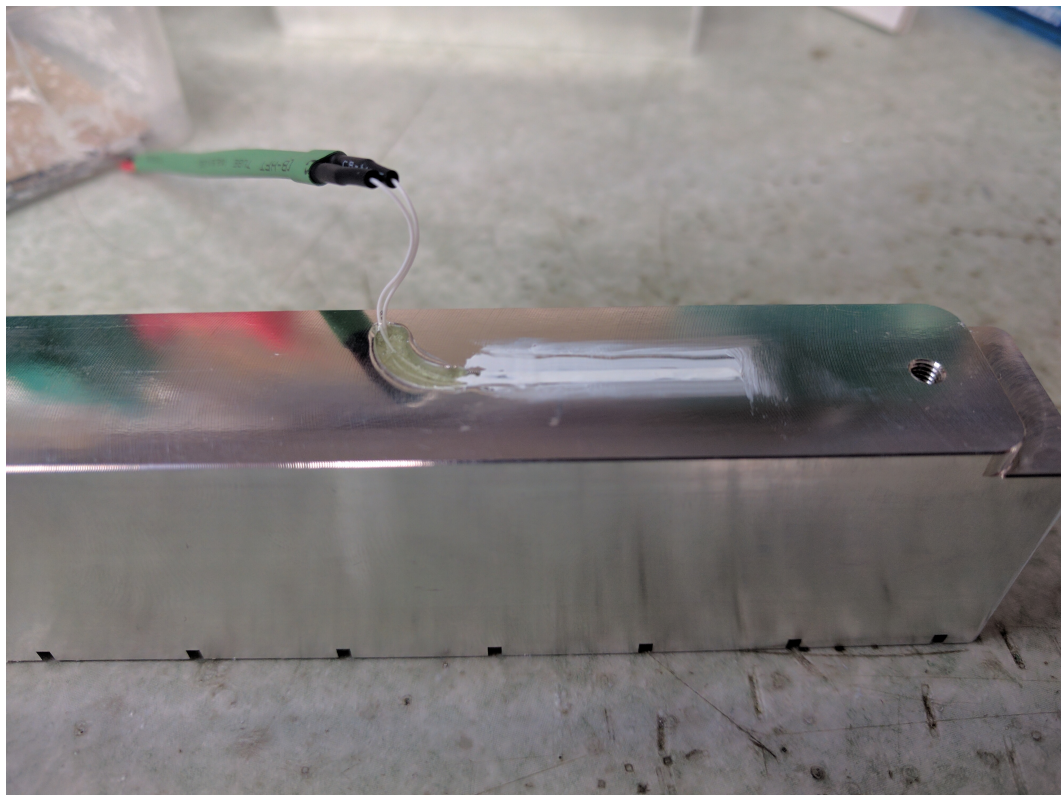


Fig. 4.14: The thermistor sensor placement in the Thermal Region.

The Thermal Region, Carrier and heat sink may now be fastened together via the two M3 bolts, with the torque specified in Section 4.1.2. The MTX Cycler electronic board is also fixed to the device and the connections for the thermistor sensor, the TEC voltage and ground along with the communications connector for the Gene-Plex Extractor main board. This assembly is shown in Figure 4.15.

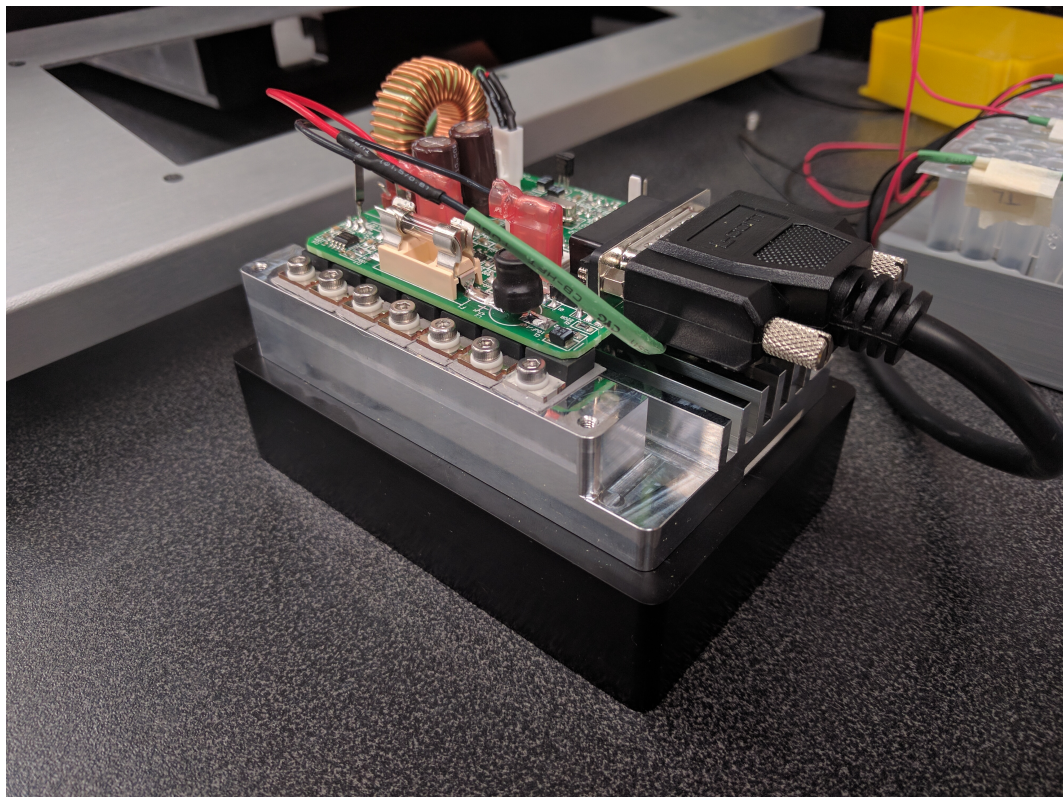


Fig. 4.15: The Thermal Region is then assembled onto the heat sink with the Carrier, along with the circuit board.

Finally, the circuit board cover may be fastened to the bottom of the module to complete the assembly. The completed Processor Module assembly is pictured in Figure 4.16.

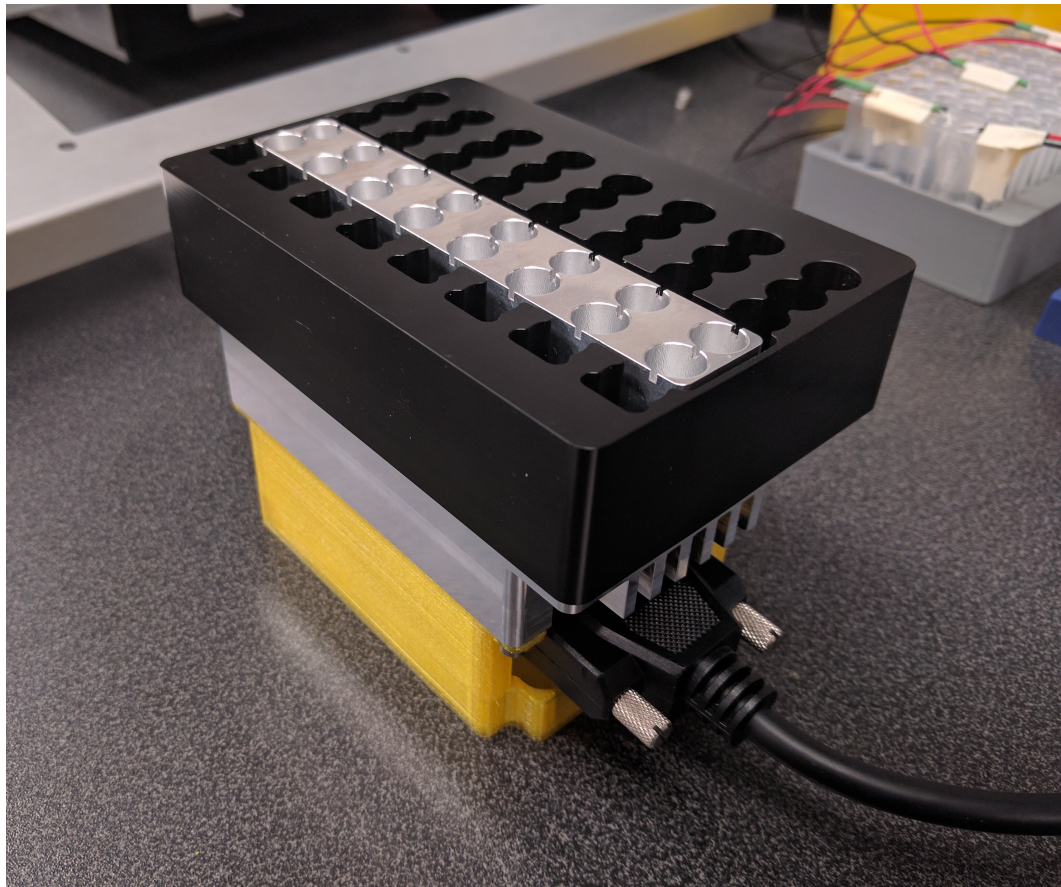


Fig. 4.16: The fully assembled Processor Module.

#### 4.1.4 Temperature Controller

Following the completion of the Processor Module hardware design and assembly, the controller design process was commenced. The results given in the following section follow the methodology presented in Section 3.1.2 to develop a PID controller along with a discrete time, Direct Designed controller.

##### Plant Identification

Using the experimental setup described in Section 3.1.2, a Processor Module was assembled for testing purposes, with the additional sensors as described. The full setup, including the Arduino interface with the thermistor

sensors, is pictured in Figure 4.17.

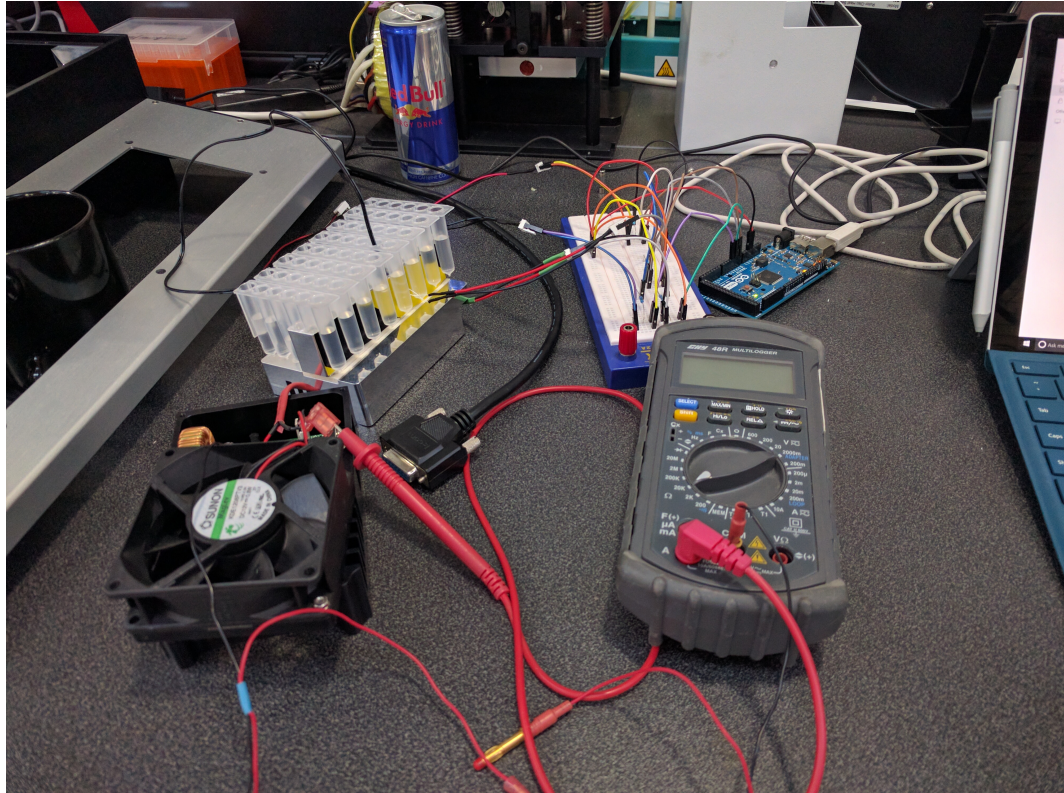


Fig. 4.17: The experimental setup used for plant identification.

The input to the system, due to the method in which the MTX Cycler electronics board functions, is PWM percentage. This PWM value determines the current which the TEC modules are driven by, at a constant 4.8 V. The value corresponding to the maximum TEC current of 8.5 A is 260 PWM units, or 26%. Therefore, the MTX Cycler software was modified to produce a constant 8.5 A at 4.8 V to provide the required step input to the system. The data collected of the systems response to this step input is displayed in Figure 4.18

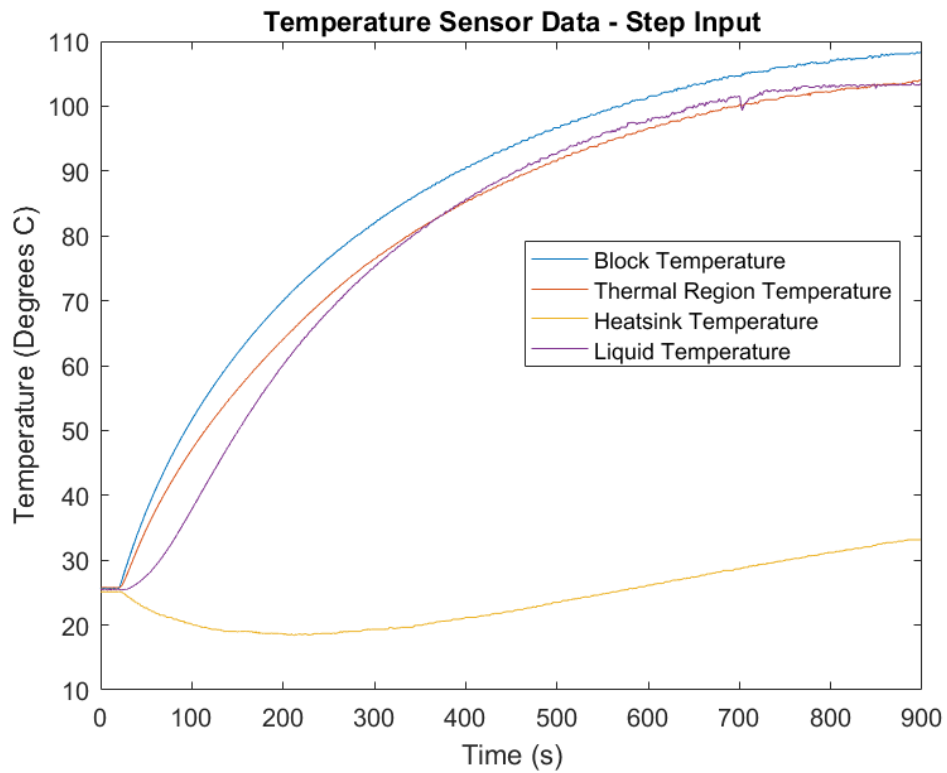


Fig. 4.18: The experimental response of the Processor Module to a step input.

The response data above includes the heat sink temperature as well as the Thermal Region temperature and liquid temperature in order to observe the response of the system. The data of interest however is the block temperature. This data is taken from the sensor installed underneath the Thermal Region, as was shown in Figure 4.14. This sensor is the source of the feedback signal to the controller to be designed, and hence is the value which will be controlled to  $60^{\circ}\text{C}$ . The isolated data from this sensor and hence the data to be used for plant identification is plotted in Figure 4.19.

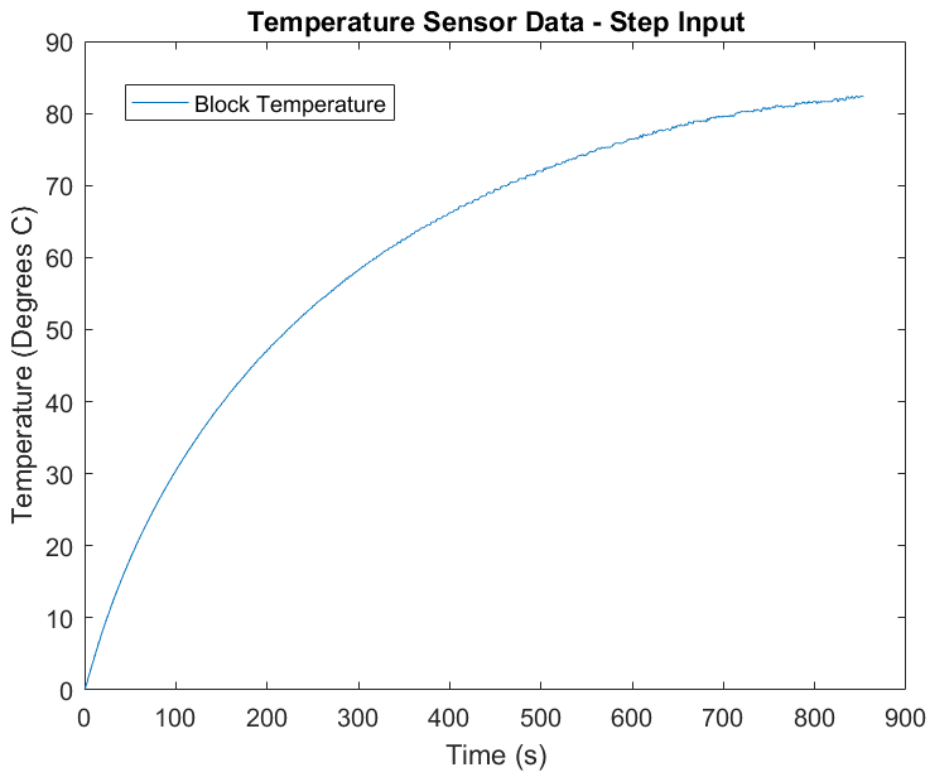


Fig. 4.19: The experimental response of the plant to a step input.

Using this data and the known step input, the MATLAB Plant Identification tool was used and the following plant identified:

$$G_p(s) = \frac{1 + 12.438s}{1 + 268.62s}$$

This single pole, single zero transfer function model was fitted to the plant response data with an accuracy of 96.47% and a MSE (mean squared error) of 0.5488.

In order to validate the plant identified, the open loop system was simulated via Simulink. The simulation was used to excite the plant with an identical 260 PWM unit step input and was compared to the experimental results. The result of this simulation is given in Figure 4.20.

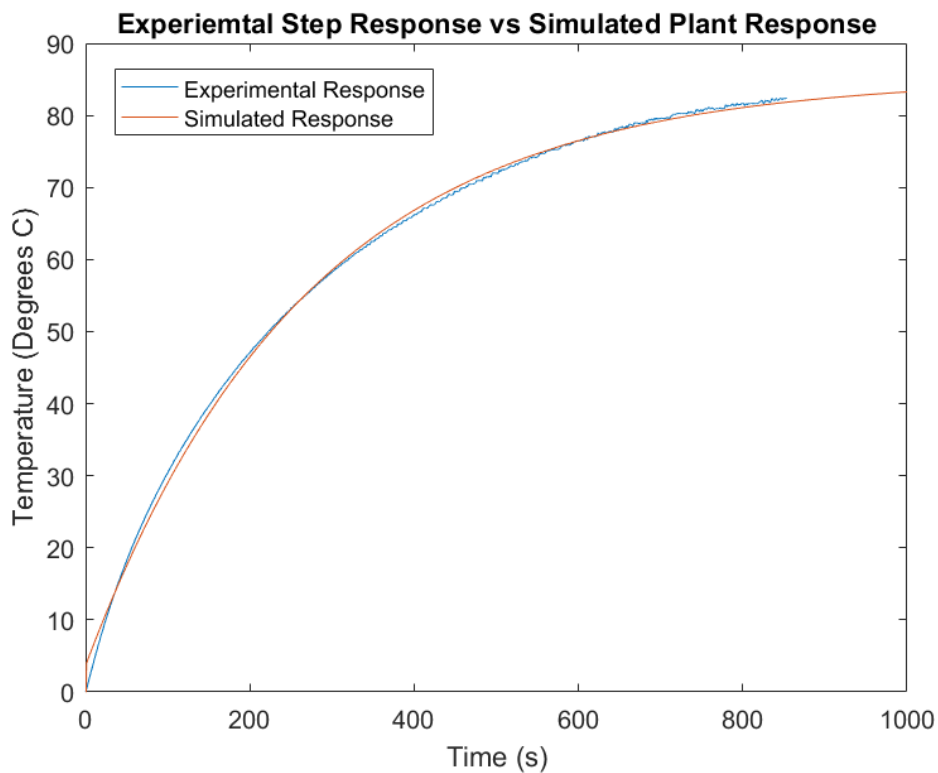


Fig. 4.20: The simulated vs experimental plant response to a step input.

### Discussion

This work has enabled the identification of the transfer function which represents the transformation carried out by the Processor Module from a PWM input to a Thermal Region temperature output. This model has been shown to fit the experimental data with a high accuracy of 96.47% and through validation produced an output fitting the experimental results to a high degree. Therefore, this plant transfer function was used for the process of controller design.

While the true output of the system is in fact the liquid temperature, it should be noted that the block temperature (temperature from the internal Thermal Region thermistor) is used for both feedback and as the controlled variable. This is due to the fact that the system which includes the liquid temperature is unobservable and hence cannot be controlled. The rate of response of the liquid temperature depends on a range of factors including the initial temperature, the liquid volume and the ambient temperature. Due to this unknown rate, the inclusion of this process in the system plant transfer function can lead to a higher degree of error in the controlled output. Due to the consistency of taking measurements and hence feedback from the internal thermistor, the output may be controlled with a high level of reliability and accuracy. Section 4.1.4 addresses the small steady state error in the liquid temperature that is a compromise of this method.

### Controller Response Requirements

The following is a concise list of requirements which must be obtained by the designed controller:

- A response time constant of 240 seconds.
- A zero steady state error, to within  $2^{\circ}\text{C}$ .
- A non-oscillatory transient response.
- An overshoot of less than  $2^{\circ}\text{C}$ .

### PID Controller Design

Using the continuous time plant transfer function identified and the MATLAB PID Tuner interface a PID controller was identified with the following values:

Proportional Gain	Integral Gain	Derivative Gain
1	80	1

Table 4.4: The PID Controller gains.

### PID Controller Verification

The designed controller was then implemented via the MTX Cycler software by modifying the C code and reprogramming the device. To record the required data for validation, the sensor layout given in Methodology Section 3.1.2 was implemented. The full experimental setup is displayed in Figure 4.21.

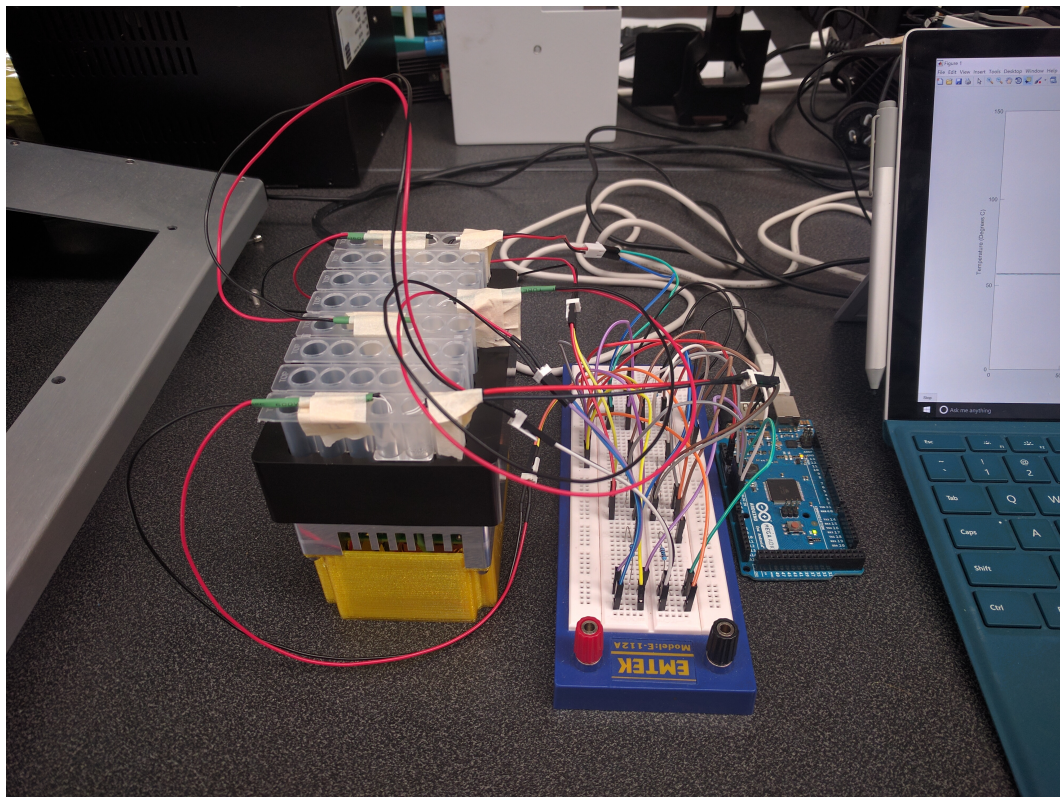


Fig. 4.21: The experimental setup utilized to experimentally verify the controller design and Processor Module.

With the reference temperature set to  $60^{\circ}\text{C}$ , the following results were obtained as plotted in Figure 4.22. The legend tube locations correlate to those displayed in Section 3.1.2, Figure 3.4.

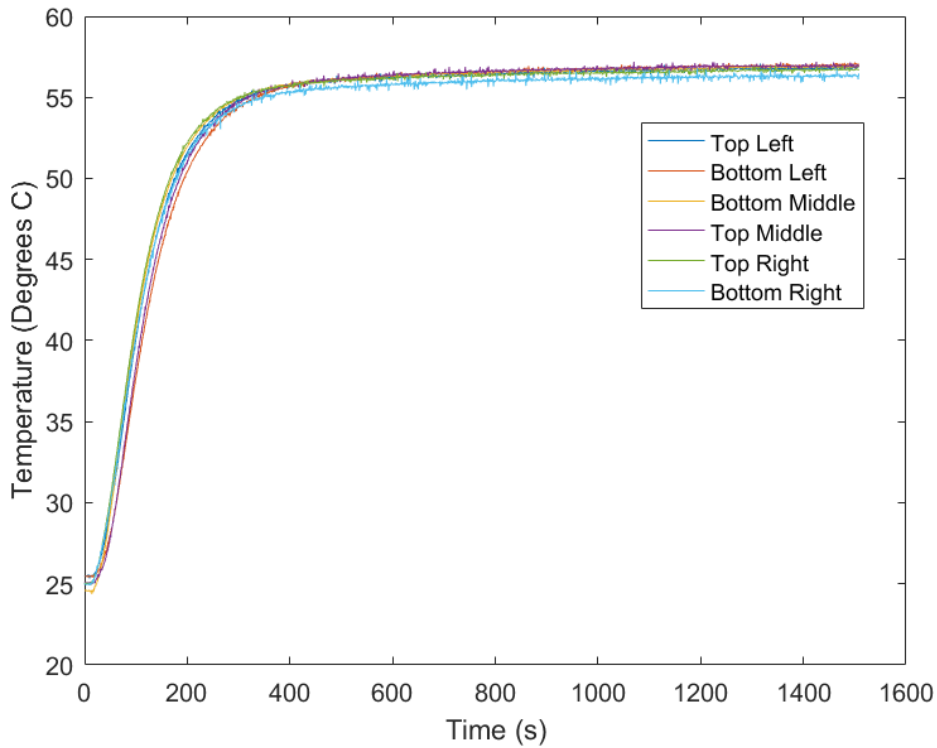


Fig. 4.22: The raw experimental data of the  $60^{\circ}\text{C}$  setpoint PID controller verification.

To gain the required information from this experimental data, a number of features were extracted. Using the mean of the steady state portion of the response, the steady state error was found to be:

$$SSE = 3.2085^{\circ}\text{C}$$

Further to this, the mean, maximum and minimum response values were extracted for the run to visualise the extreme temperatures experienced across the measured tubes. This data is plotted in Figure 4.23.

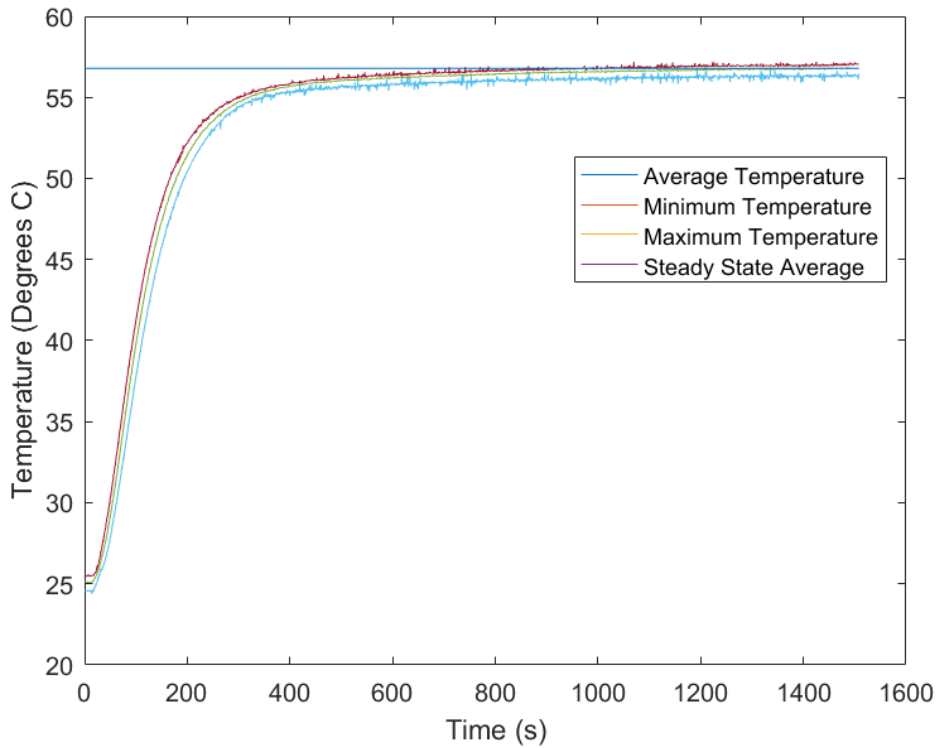


Fig. 4.23: Key experimental data of the 60°C setpoint PID controller verification.

### Discussion

The experimental results obtained show a number of key points regarding the controller designed. The controller response shows a time constant of 81.16 seconds, with a steady state error of 3.2085 °C. While the time constant achieved exceeds the system requirements, the systems steady state error does not fall within the acceptable range. As was noted earlier, this was an expected outcome due to the use of the internal Thermal Region sensor as the feedback value and controlled output variable. Therefore losses that occur as heat energy is transferred from the TEC modules, through the Thermal Region and cassette tubes and finally into the liquid are accumulated in the steady state error observed. This however has allowed for the high degree of stability observed. In order to rectify this error, a calibration

process is used, where the error observed is applied directly to the system reference signal in order to achieve the steady state response required of the system. This calibration process allows for stable and consistent controller performance along with the ability to achieve the required steady state error of the system with minimal effects of system disturbances

### Controller Calibration

With the previous results showing the transient response of the controller to meet system requirements yet an unacceptable steady state error, the observed error was used to offset the reference signal and the Processor Module reprogrammed. The results of this calibrated experiment are plotted in Figure 4.24.

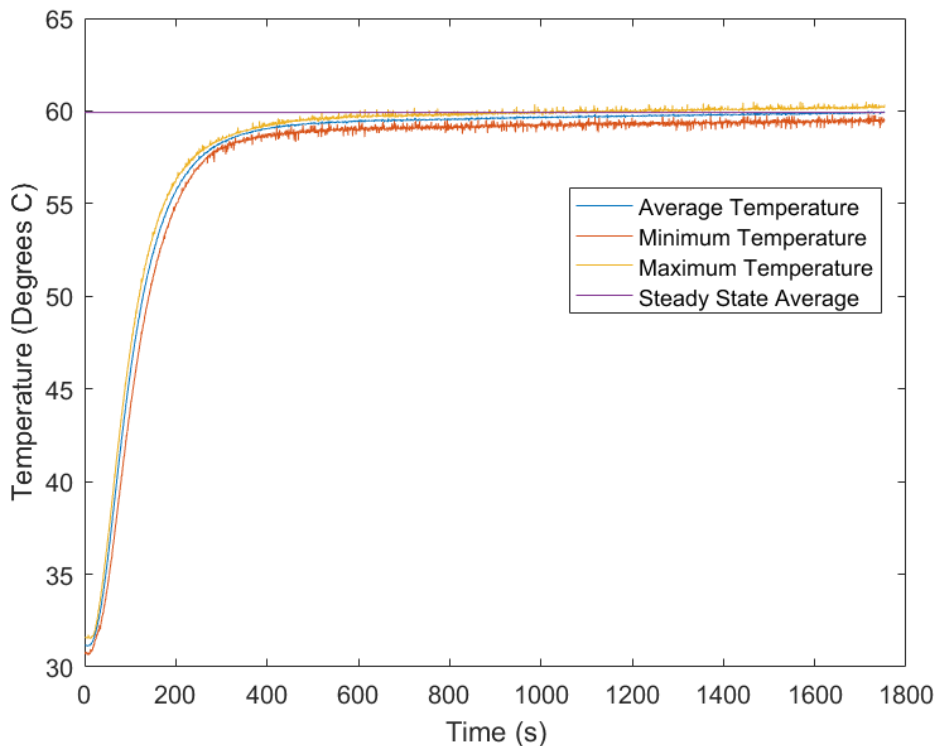


Fig. 4.24: Key experimental data of the calibrated  $63.2^{\circ}\text{C}$  setpoint PID controller verification.

Once again using the mean of the steady state portion of the response, the steady state error was found to be:

$$SSE = 0.083^{\circ}\text{C}$$

### Discussion

As was observed in Figure 4.24, the calibrated response of the controller corrects the steady state error issues observed in previous results. Furthermore, the time response along with the zero overshoot transient response has been maintained as required. Furthermore, the system has demonstrated a stable long term response, with the temperature reaching the controlled steady state value and remaining stable for a total period of 30 minutes. Not only does this verify the performance of the designed PID controller, it also verifies the success of the mechanical design. The ability of the system to reach and maintain a steady state temperature indicates the stability of the thermal design of the system. Therefore, the success of this experiment has allowed both the PID temperature controller along with the Processor Module design itself to be experimentally verified.

### Discrete Time, Direct Method Controller Design

Following the successful design and verification of the PID controller and the Processor Modules thermal stability, the design of the discrete time controller was commenced. The following results follow the method described in Section 3.1.2.

With the plant transfer function already identified and verified, the dis-

October 24, 2016

crete time equivalent was found to be:

$$G_p(z) = \frac{0.01518 - 0.01457z^{-1}}{1 - 0.9981z^{-1}}$$

This plant was derived from the plant identified in Section 4.1.4, Plant Identification, and uses a sample time of  $T = 0.5\text{s}$ . The pole zero map of this discrete time transfer function is plotted in Figure 4.25.

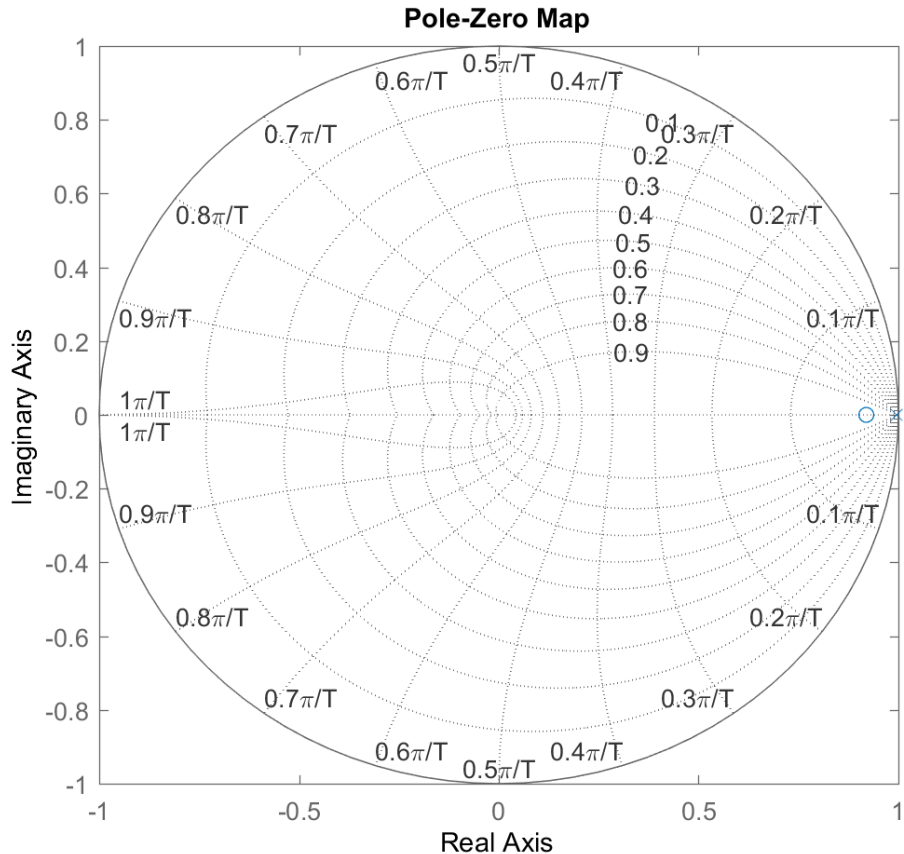


Fig. 4.25: The pole zero map of the discrete transfer function of the Processor Module plant.

In order to form  $F(z)$ , the desired time response of the controller was

then set as  $\tau = 250$ s. This gives an s-domain pole location of:

$$s = -\frac{1}{250}$$

Which corresponds to the z-domain pole of:

$$z = 0.9979$$

Therefore,  $F(z)$  becomes:

$$F(z) = \frac{b_0}{z - 0.9979}$$

Applying stability constraints 1 and 2, the Pole-Zero map in Figure 4.25, it is seen that there are no unstable poles or zeros present in the system. Therefore,  $F(z)$  does not require any additions to prevent unstable cancellations by the controller.

Checking the causality constraint,  $D(G_p(z)) = n = 0$  and  $D(F(z)) = m = 1$ . Since  $m > n$ , the controller is strictly proper and no time delays were required.

Applying the steady state error requirement:

$$F(z)|_{z=1} = F(1)$$

$$b_0 = 0.0021$$

Therefore, the final form of  $F(z)$  is:

$$F(z) = \frac{0.0021}{z - 0.9979}$$

This results in the following discrete controller transfer function:

$$G_c(z) = \frac{0.0021z^{-1} - 0.004195z^{-2} + 0.002095z^{-3}}{0.01518 - 0.04495z^{-1} + 0.04436z^{-2} - 0.01459z^{-3}}$$

And the final difference equation to be implemented of:

$$\begin{aligned} m(k) = & 2.9611m(k-1) - 2.9223m(k-2) + 0.9611m(k-3) \\ & + 0.1383e(k-1) - 0.2764e(k-2) + 0.1380e(k-3) \end{aligned} \quad (4.10)$$

### Discrete Time, Direct Method Controller Validation

Following the design of the discrete time controller, it was modelled via Simulink in order to verify its' performance. The results of this simulation are provided below in Figure 4.26.

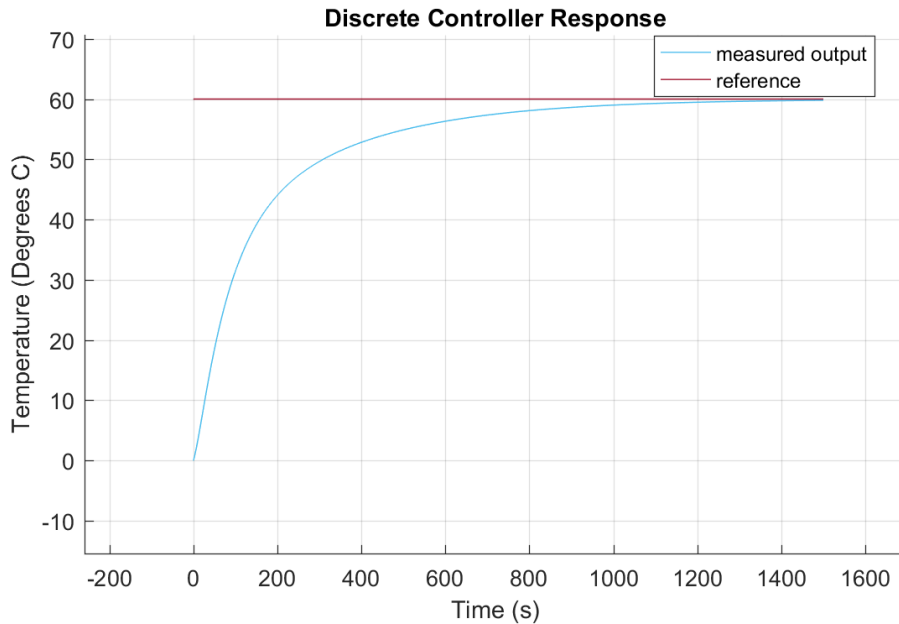


Fig. 4.26: The simulated response of the designed discrete controller.

**Discrete Time, Direct Method Controller Verification**

The controller was then implemented via a C function within the MTX Cycler software in the form of the difference equation of Equation 4.10. The function implemented is given below:

```
void TemperatureControl( void )
{
    if( settemperature > 0)
    {
        //Shift errors back
        e3 = e2;
        e2 = e1;
        e1 = e;
        //Shift controller efforts back
        m3 = m2;
        m2 = m1;
        m1 = m;
        //Calculate error
        e = (float)settemperature - (float)temperature;
        //Calculate controller effort
        m = c1*m1-c2*m2+c3*m3+c4*e1-c5*e2+c6*e3;
        pwmdrive = (short)m;
        //set bridge direction
        if( pwmdrive > 0){
            BRIDGE_HEAT;
        } else {
            BRIDGE_COOL;
        }
    }
}
```

```
        }

        //Correct after direction change
        if (pwmdrive < 0) pwmdrive = -pwmdrive;

        //Limit maximum drive
        if (pwmdrive > MAXDRIVE) pwmdrive = MAXDRIVE;
    } else {
        // no temp control enabled
        //limit turn off rate of pwm
        pwmdrive = 1023 - OCR1A;
        if (pwmdrive > DELTAPWM){
            pwmdrive = pwmdrive - DELTAPWM;
        } else {
            pwmdrive = 0;
        }
    }

    // drive updated in current limit routine
    pwmout = pwmdrive;
}
```

## Discussion

The results of this implementation however encountered a persistent issue. The response of the controlled temperature was observed to cycler between heating and cooling action in a repetitive loop which did not cease or deviate. After measuring the current which was being supplied to the TEC modules as a result of the controller, it was noticed that this value would

cycler between maximum current and minimum current in the same fashion. By observing this response, it was hypothesised that a data overflow was occurring within the control function. Efforts to debug this issue were hindered by the lack of debugging on the Atmel ATmega16 used for the MTX Cycler electronics. Therefore, only simulated debugging environment was available. Despite significant efforts to locate the source of the error, due to time constraints the issue was not resolved. Despite this, the validation simulation conducted provides evidence that the controller design was indeed successful. It is therefore able to be implemented as part of the debugged software as future work.

#### 4.1.5 Magnetic Separation

With the mechanical design and thermal control elements integrating into the Processor Module, the magnetic separation capabilities were considered. The first stage of this process involved consideration of the various magnetic configurations and arrangements which may be used. As was noted in Chapter 2, Literature Review, this investigation focused on the Neodymium composition specifically.

Three main magnet configurations were considered for application in this component. The first was the arrangement of one or more geometrically simple magnets, as available from common suppliers. Such an arrangement is simple to assemble, cost effective and relatively high strength. They also allow an ideal position to be created to ensure full magnetic field coverage of the pipette tip.

Also considered was the use of a magnetic circuit. These devices use a ferromagnetic material to redirect the magnetic field of the magnet. Such a circuit may be used to redirect the magnetic field to a specifically sized air gap, at which point the concentrated magnetic field may in fact be of greater strength than that provided by the magnet [28].

The final considered arrangement was the Halbach Array. These array use a strategic positioning and orientation of small magnet elements to manipulate the magnetic field. The result is a field manipulation such that only one side of the magnetic arrangement experiences a magnetic field. This effect is visualised in Figure 4.27.

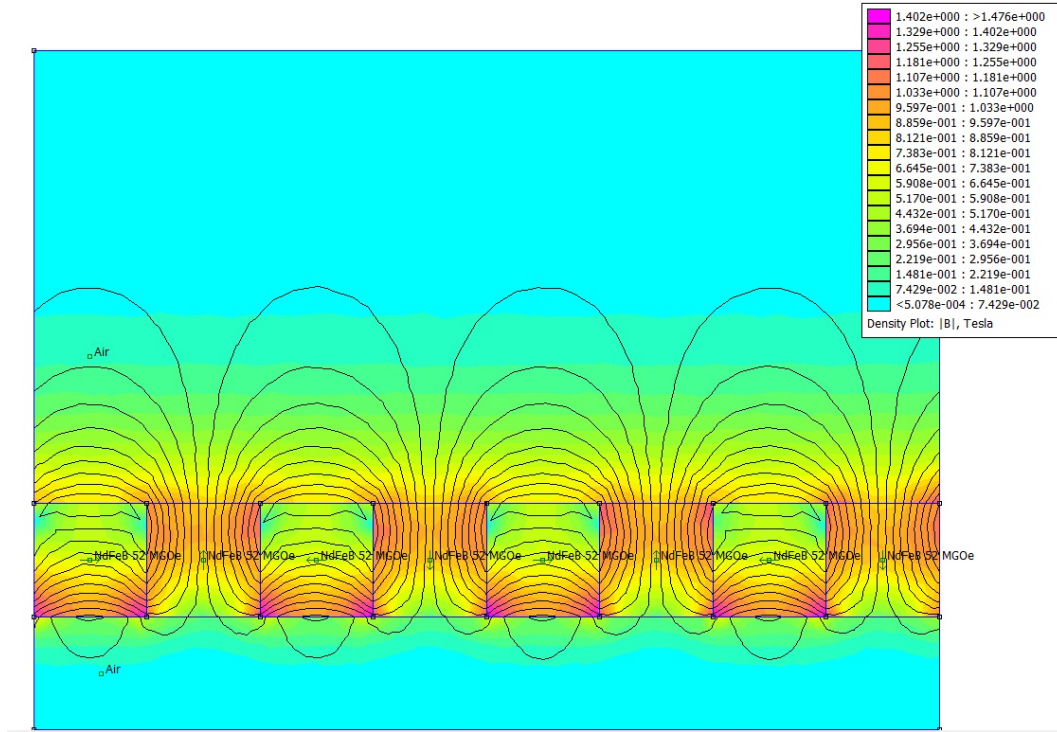


Fig. 4.27: Halbach Array Flux Diagram.

Such an arrangement has a number of potential benefits. Firstly, the ab-

sence of magnetic field on one side of the arrangement may be beneficial in ensuring other magnetic elements of the Gene-Plex Extractor are not effected. Furthermore, these arrangements have been shown to produce up to two times the magnetic field strength of the combined magnetic elements on the directed side.

In order to determine the feasibility of such an arrangement, a representative test piece was created via 3D printing. The array created, pictured in Figure 4.28, allowed the testing of 3 differing halbach array configurations.

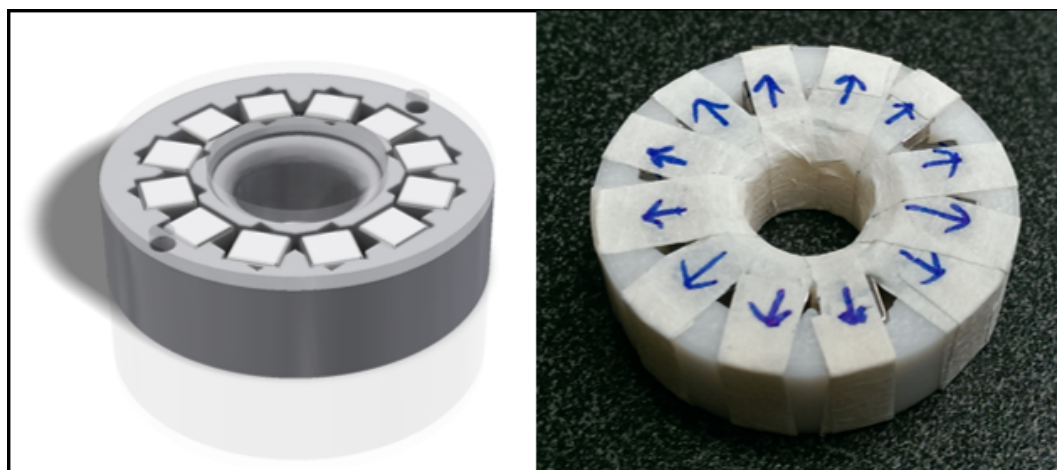


Fig. 4.28: Halbach Array Test Jig. [?]

Of the three configurations tested, the arrangement known as "k=1" was experimentally shown to be the most effective, as is seen in Figure 4.29.

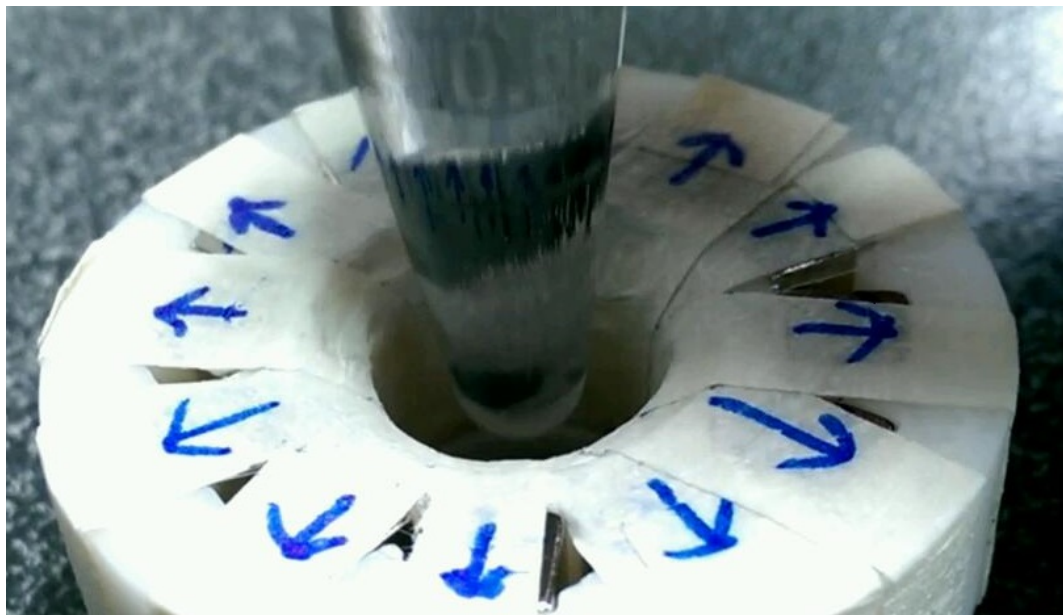


Fig. 4.29: Halbach Array Test Jig for K=1.

Despite the experimental evidence showing the effectiveness of the array, it was decided an inefficient means of achieving the required separation. This was due to the high level of complexity and hence assembly effort, the cost of the  $12\ 5mm^3$  magnet elements required by each array and the relatively marginal benefits provided over the simple magnetic block arrangement. Therefore, as a result of this investigation, it was concluded that a simple magnetic block arrangement is the most effective method for achieving the separation of the magnetic silica beads.

This conclusion was applied and the resulting design, pictured in Figure 4.30 produced. This figure shows the resulting placement of the magnetic blocks within the tube location of the Carrier, where the magnetic fields of each magnet are aligned to create a uniform magnetic field.

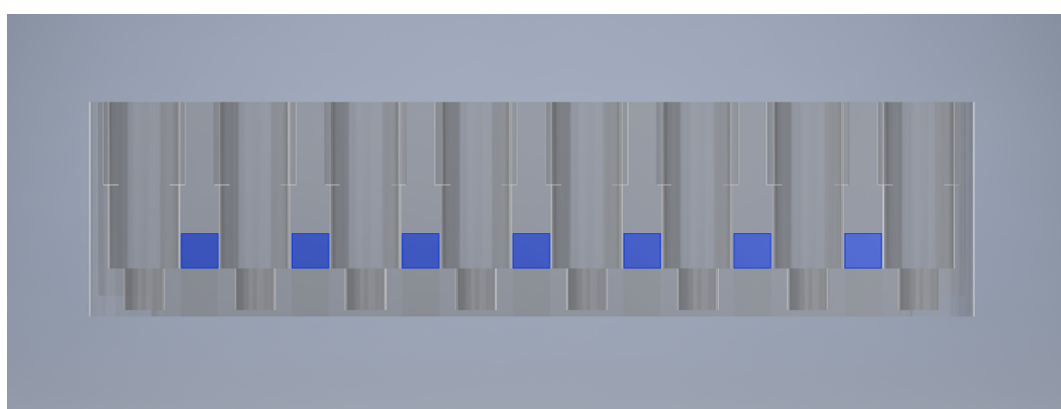


Fig. 4.30: The positioning of block magnets between the liquid tubes for the Processor Module magnetic separation.

# Chapter 5

## Conclusions

This work has developed the required additions to the Gene-Plex Extractor platform, enabling the functionality of several key capabilities for the extraction of DNA/RNA via super paramagnetic bead based extraction.

It was discovered that the use of an air gap along with significant reduction in surface area contact, provides adequate levels of thermal insulation. Paired with the minimization of the heated mass and a heat sink of ample capacity, this setup was found to provide a stable platform for temperature control. This platform was found to be capable of sustaining a set temperature of 60°C for an experimentally tested 30 minute period, where no degradation of the system was found. Therefore, it is concluded that the design methodology used has enabled the creation of a thermally stable system.

Furthermore, it was shown via numerical simulation and experimental verification that the TEC module is an effective means of providing the heat energy necessary to maintain the system at the required setpoint. Not only were the devices used capable of driving the system to the required thermal

state, however the rate of response achieved exceeds the requirements of the component. Along with their high degree of reliability and high MTBF, the device selected for this application is concluded as an effective solution.

The PID controller implemented has been verified as a suitable means of controlling the temperature of the system. Despite the simplified design method and the lower degree of control, the controller designed was capable of driving the system to a steady state in the required time period, with the transient response required. This response exhibited a stable steady state response over a long term experiment. Therefore it has been shown that the developed PID controller is an effective controller for the system designed.

While the discussed PID controller achieved the stable steady state required, it is noted that the zero error condition is not inherently met. As was discussed, this is due to the design decision to take temperature feedback measurements from a location as close to the TEC module heating elements as possible. This decision has been shown through the response to result in the required transient response being achieved, however it is evident that the thermal losses occurring in the system result in an error at the liquid temperature as the temperature of interest. This temperature error was however shown to be stable, and may therefore easily and reliably be corrected via a simple calibration. This calibration was in the form of a temperature offset equal to that of the steady state error, and resulted in a corrected response with the liquid temperature achieving an error of only  $0.083^{\circ}\text{C}$ . Due to this result, this calibration process along with the placement of the temperature sensor may be concluded an effective control strategy.

The design of the discrete time, direct analytical method controller was completed and validated. The design of the controller was shown via simulated response to exceed the requirements of the system and control the system to a zero error steady state, with the stipulated transient response. Despite the successful validation of the controller design, the implemented software controller was not able to be verified due to the data overflow bug described. Despite this shortcoming, it may however be concluded via the simulated validation that the developed controller is capable of meeting and exceeding the system requirements.

Finally, via a review of the applicable magnetic configurations and arrangements, the use of the simple block magnet was found to be most effective for use in this application. This was due to the high strength of the ND-B-Fe magnet chemistry and the unnecessary complexities of the investigated arrangements which were found experimentally to give negligible advantage. Therefore, pending further experimental validation and verification, it is concluded that the application of simple, high strength ND-B-Fe magnets is the most effective option for further work.

# Chapter 6

## Future Work

In order to complete the full set of required capabilities for the commercial viability of the Gene-Plex Extractor, as outlined in Chapter 1, this work shall be furthered. This includes the full development of the magnetic separation capabilities and their verification, the implementation of a hygeinic waste disposal method and the addition of the required routines to the platforms software.

Further to this, further work is required in order to fully realise the implemented discrete time controller. Such work includes the full debugging of the developed control routine in order to identify the source of the currently experienced data overflow. Following successful debugging, the fully implemented controller must be validated using an experimental setup identical to that employed in Section 4.1.4. This must be conducted to ensure the response of the controller achieves the required system performance and the transient response is as expected from the Simulink simulation conducted.

# Bibliography

- [1] Honghua Liao. Simulations research on smith predictive adaptive fuzzy-pid compound controller in the temperature control system of microchip level pcr instrument. *Applied Mechanics and Materials*, 373-375:1324 – 31, 2013//.
- [2] Rym Kefi, Bertrand Mafart, Jean Louis Spadoni, Alain Stevanovitch, and Eliane Beraud-Colomb. Real-time polymerase chain reaction (pcr) for the study of ancient dna. *Comptes Rendus - Palevol*, 2(2):125 – 132, 2003.
- [3] J.E. Edwards and D.W. Otterson. Tech talk: (5) temperature measurement basics. *Measurement and Control*, 47(9):276 – 82, 2014/11/.
- [4] Jing Huang, Zhangwei Chen, and Kewei Hu. Fea for steady-state thermal performance of pcr thermal-cycler based on thermoelectric cooler. volume vol.2, pages 1097 – 100, Piscataway, NJ, USA, 2011//. steady state thermal performance;PCR thermal cycler;thermoelectric cooler;polymerase chain reaction;PCR technology;DNA sequence;periodic heating;cooling;finite element model;multistage TEC;ANSYS Workbench 12.0;TEC XLT2389 and;.
- [5] R. Shirafkan, M.M. Abdevand, M. Ghanbari, O. Shoaei, and M.J. Yazdanpanah. Design and implementation of a nonlinear controller for

- thermal cycler with application to dna amplification. *Transactions of the Institute of Measurement and Control*, 38(3):293 – 304, 2016.
- [6] John R. Widomski, Adrian Fawcett, Douglas E. Olsen, Richard W. Nor eiks, Charles M. Wittmer, Paul M. Hetherington, John G. Atwood, and Keith S. Ferrara. Thermal cycler for pcr. 11654239(20070113880), 2007/05/24.
- [7] Ferrotec Corporation. Thermoelectric Module basics, 2015.
- [8] Bijan Karimpourian and Jafar Mahmoudi. Some important considerations in heatsink design. volume 2005, pages 406 – 413, Berlin, Germany, 2005.
- [9] B. Baudouy. Heat transfer and cooling techniques at low temperature. pages 329 – 352, Erice, Italy, 2014.
- [10] Fenton Williams, Albert Carmelo Mossa, Lisa May Goven, Timothy M. Woudenberg, Richard Leath, Marcel Margulies, John Girdner Atwood, Clive Miles, and Robert P. Ragusa. Thermal cycler for automatic performance of the polymerase chain reaction with close temperature control. 10691186(7238517), 2007/07/03.
- [11] John R. Widomski, Adrian Fawcett, Douglas E. Olsen, Richard W. Nor eiks, Charles M. Wittmer, Paul M. Hetherington, John G. Atwood, and Keith S. Ferrara. Thermal cycler for pcr. 11654239(20070113880), 2007/05/24.
- [12] Carl T. Wittwer. System and methods for monitoring pcr processes. 05020549.1(1704922), 2006/09/27.

- [13] Luis E. Vilchiz-Bravo, Arturo Pacheco-Vega, and Brent E. Handy. Sensor placement in temperature-based control strategies to improve baseline stability in tian-calvet microcalorimeters. *Journal of Thermal Analysis and Calorimetry*, 111(1):857 – 867, 2013.
- [14] P. OLAFSSON, R. SANDSTROM, and Å KARLSSON. Comparison of experimental, calculated and observed values for electrical and thermal conductivity of aluminium alloys. *Journal of Materials Science*, 32(16):4383–4390, 1997.
- [15] A. Balraj, A. Patvardhan, V. Renuka Devi, R. Aiswarya, and V. Prasen. Embedded temperature monitoring and control unit. pages 293 – 7, Piscataway, NJ, USA, 2010//.
- [16] P. Welander. Challenges of temperature sensing. *Control Engineering*, 55(12):41 – 2, 2008/12/.
- [17] A. Cellatoglu and K. Balasubramanian. Assessment of the dynamic performance of process control systems: A case study with temperature controller. volume vol.4, pages 19 – 23, Piscataway, NJ, USA, 2011//.
- [18] Rare earth magnets: Making the world a better, faster, safer place. *Industrial Heating*, 73(4):28 – , 2006.
- [19] S.S. Shevkoplyas, A.C. Siegel, R.M. Westervelt, M.G. Prentiss, and G.M. Whitesides. The force acting on a superparamagnetic bead due to an applied magnetic field. *Lab on a Chip*, 7(10):1294 – 302, 2007/10/.
- [20] C. Mikkelsen and H. Bruus. Microfluidic capturing-dynamics of paramagnetic bead suspensions. *Lab on a Chip*, 5(11):1293 – 7, 2005/11/.

- [21] Associate Professor Jay Katupitiya. Design of Controllers direct methods, 2015.
- [22] Sorenson Engineering. Personal Communication.
- [23] MMT Observatory. Fits and tolerances, 2015.
- [24] Ferrotec Corporation. Thermoelectric Module basics, 2015.
- [25] Ferrotec Corporation. Thermoelectric Module Modelling, year = 2015, url = <https://thermal.ferrotec.com/technology/thermoelectric-reference-guide/thermalref11/>, urldate = 2016-9-1.
- [26] British Standard. BS EN 61010-1:2010. Technical Report 10.
- [27] Jehbco. Sponge silicone sheet, 2015.
- [28] MIT. Magnetic circuits, 2011.

# Appendix A

## CFD Simulation Convergence

### Data

Figure A.1 shows the convergence plot for the refined, 2 TEC design simulation.

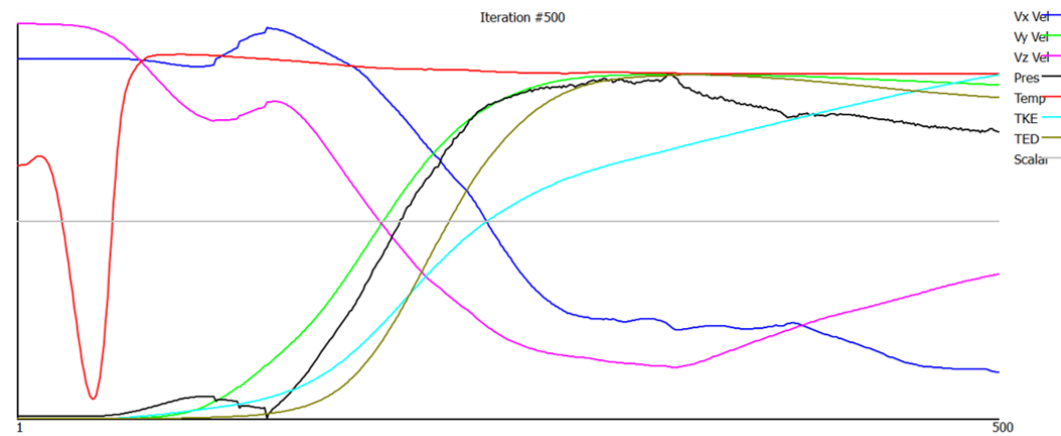


Fig. A.1: Convergence Plot for Refined Design CFD.